

1 **The October 29, 2018 storm in Northern Italy – an exceptional event and its modeling**

2
3 L.Cavaleri^{1*}, M.Bajo¹, F.Barbariol¹, M.Bastianini¹, A.Benetazzo¹, L.Bertotti¹, J.Chiggiato¹,
4 S.Davolio², C.Ferrarin¹, L.Magnusson³, A.Papa⁴, P.Pezzutto¹, A.Pomaro¹, G.Ungiesser¹

5
6 1 – CNR-ISMAR, Venice, Italy
7 2 – ISAC, Bologna, Italy
8 3 – ECMWF, Reading, U.K.
9 4 – CPSM, Venice, Italy

10
11 *) reference author: luigi.cavaleri@ismar.cnr.it

12 ISMAR
13 Arsenale – Tesa 104
14 Castello 2737/F
15 30122 Venice, Italy
16 ph +39-041-2407-955

17
18
19
20
21
22
23
24
25
26
27
28
29
30
31
32
33
34
35
36
37
38
39
40
41
42
43
44
45
46
47
48
49

25 March 2019

50	Keywords:
51	storm
52	extreme conditions
53	cyclogenesis
54	wind waves
55	coastal processes
56	storm surge
57	
58	

59

Abstract

60

61

62 On October 29, 2018 a very severe storm affected Northern Italy, and in particular the Adriatic Sea.
63 The ensuing surge and wave conditions at and in front of Venice stand at the far tail of the
64 respective historical distributions. The large set of available measured data, at the coast and at the
65 offshore oceanographic tower, coupled with detailed numerical simulations, allows a keen analysis
66 of the storm, its predictability and in particular of the ensuing enhanced coastal processes. These
67 include the coastal set-up, the input information for tidal prediction in Venice, the documented
68 passage of an atmospheric cold front and, using the local tidal data, the derived possibility of
69 estimating of the surface wind stress, the evidence of reflected waves from the coast and the
70 associated seismometers signal 40 km inland. The highest crest and wave heights measured at the
71 tower are beyond what suggested by non-linear statistics. The relative out-of-scale of the three
72 major storms since 1966 suggests the possibility that they belong to a self-standing family of
73 events.

74

75

76 **1 – Introduction**

77 The storm we consider in this paper developed at the end of October in the Western Mediterranean
78 Sea as an explosive cyclogenesis following a cold input from the Gulf of Lion (see Figure 1 for the
79 geographical references). Born West of Sardinia, the ensuing very compact low deepened rapidly
80 moving at high speed toward North. The low forced strong winds on its right flank that led to
81 destructive (compared to the local standards) waves in the Ligurian Sea. At the same time the low
82 led also to a very strong South-East sirocco wind in the Adriatic Sea, with consequent high waves in
83 front of Venice and a substantial surge that only by a lucky chance did not happen to be by far the
84 worst in documented history. In this paper we analyze the storm, focusing our attention on the
85 Adriatic events. The evolution of the storm, located on the tail of the related historical distribution,
86 led to peculiar conditions in front of Venice, conditions that, thanks to the extensive measurements
87 available at the coast and at the CNR-ISMAR (henceforth ISMAR) oceanographic tower (15 km
88 offshore), pushed us to go deeper into the physics of coastal processes. The abundance of data and
89 the extensive modeling allow discussing in sequence several different aspects of the storm. With
90 this background the paper is organized as follows.

91

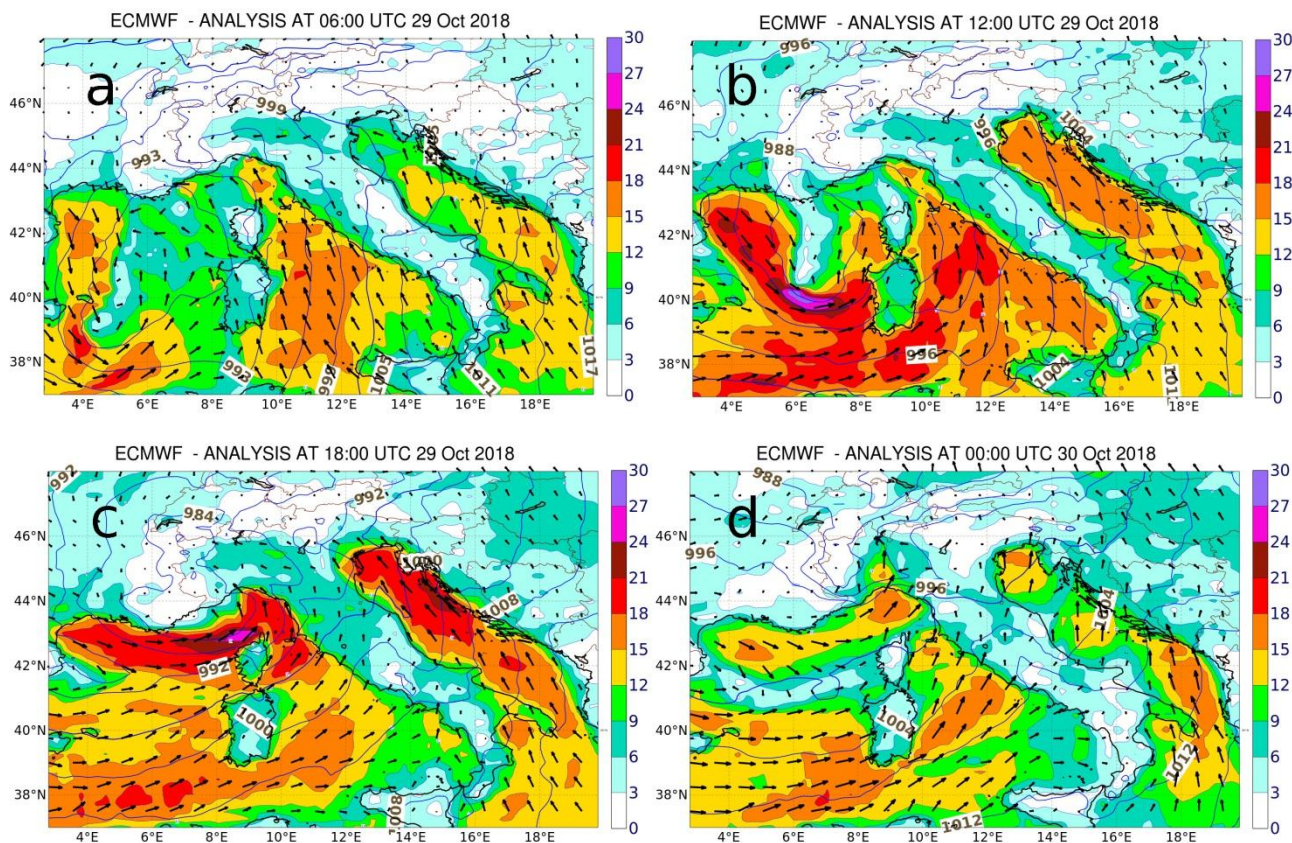


92

93 Figure 1 – Western and central Mediterranean Sea. The main geographical features and the relevant
94 locations are indicated. The lines show respectively: A) the path and timing of the cyclogenesis
95 minimum, B) the direction of the strong winds associated with it, C) the direction of the sirocco
96 winds on the Adriatic Sea, D) the path followed by the violent cold front. The small rectangle on
97 Venice indicates the area enlarged in Figure 3.

98

99 Section 2 provides a comprehensive, although compact, description of the meteorology of the
 100 storm, what was peculiar in it, and its various severe aspects. Focusing mainly on the Adriatic Sea,
 101 Section 3 lists the available measured data, both from the local sources and by remote sensing. The
 102 general modeling approach, covering meteorology and oceanography, the latter both as waves and
 103 surge (implicitly circulation), is given in Section 4. In Section 5 we report and discuss the
 104 corresponding model results. Being the heart of the paper, this section is more extended than the
 105 other ones, going into the details of the basic cited parameters, i.e. wind, waves and surge. The non-
 106 negligible aspect of predictability is dealt with in Section 6, leading also to an interesting
 107 comparison with the two similar storms of 1966 and 1979. In Section 7 we go more into the physics
 108 of coastal processes taking advantage of the contemporary availability of data at the coast and at the
 109 tower position, 15 km offshore. In Section 8 we zoom on the conditions at the tower and try to
 110 relate the possible extremes derived from the wave model spectra with the ones available from
 111 direct records and deduced from the damages on some over-structures of the tower. The statistical
 112 significance of the storm is assessed in Section 9 as derived from the long term records available on
 113 board. All this is critically discussed in Section 10 where we point out the successes, but, most of
 114 all, the small and not so small errors of the models, deriving, or at least discussing, where problems
 115 may lie and improvements are required. All this is itemized in the final Section 11.



116
 117 Figure 2 – Surface wind speed (ms^{-1}) and surface pressure fields on the Western Mediterranean Sea.
 118 The four panels show the ECMWF analysis at respectively (UTC time of 29 and 30 October 2018):
 119 a) 06-29, b) 12-29, c) 18-29, d) 00-30.

120

121 **2 – The meteorological evolution of the storm**

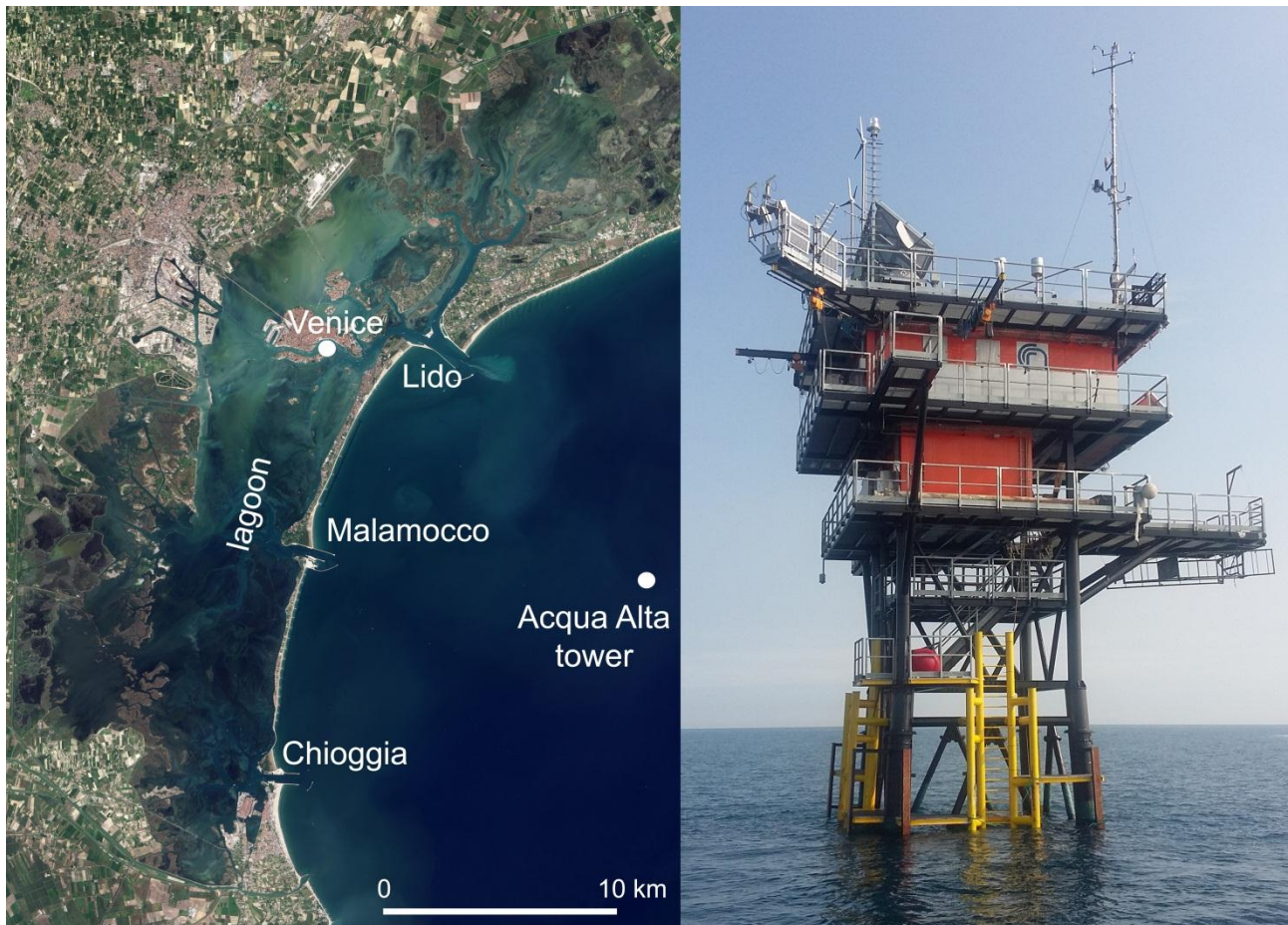
122 In late October 2018 the synoptic characteristics of the weather conditions over the Western
123 Mediterranean Sea resembled the typical pattern associated with major rain events over the southern
124 side of the Alpine range. A large scale cyclonic system was slowly evolving leading to southerly
125 flow towards the Alps (see Figure 1 for the geography of the area), with consequent intense alpine
126 precipitation events. At the surface the wind over the sea was oriented from South-East in the form
127 of a low level jet over both the Tyrrhenian and Adriatic seas, respectively to the West and East of
128 Italy. After a short break, a second and more intense phase of the event took place on the 29, when a
129 cold front from the Gulf of Lion entered the Mediterranean basin (panel 2a, at 06 UTC). The
130 interaction between the cold inflow with the warm and moist marine boundary layer triggered the
131 rapid intensification of the minimum that, starting from the general field, quickly underwent (12
132 UTC, panel 2b) an explosive cyclogenesis down to 984 hPa. The cyclone moved rapidly northwards
133 (A in Figure 1; note timing of its sequential positions) while still deepening down to 977 hPa (U.K.
134 Meteorological Office) and further contracting its horizontal scale. Moving North, the low forced
135 strong south-easterly winds on its right flank, both on the Tyrrhenian Sea (B in Figure 2, with the
136 flow squeezed between the low and the Apennines range along the peninsula) and the Adriatic Sea
137 (C, here enhanced by the high pressure over eastern Europe). The winds led to high waves both on
138 the Ligurian Sea and the Northern Adriatic Sea. The low entered land north of Corsica at about 18
139 UTC, followed (D) by a strong and violent flow of cold air from West-South-West (panel 2c, 18
140 UTC). This very energetic cold flow quickly passed over the Apennines, precipitating into the
141 Adriatic basin. In a way this halted the flood of Venice, but, forcing the sirocco wind into a
142 narrower path against the Eastern Alps, it also led to tremendously strong winds on the mountain
143 area (Dolomites and Eastern Alps), with record wind speeds (gusts up to 213 kmh^{-1} recorded before
144 the instrument flew off) and very extensive forest damage (the estimated loss is of 11 million
145 trees). On the Adriatic Sea, where we focus our attention, the wind was over at 00 UTC of the 30th
146 (panel 2d), while of course the long swell was still pounding on the Venetian coast.

147

148 **3 – The observational dataset**

149 Figure 3 provides the geometry of the Venetian coast (area marked in Figure 1) and a view of the
150 ISMAR oceanographic tower “Acqua Alta” (literally “high water”, a superstitious name following
151 its construction after the big flood of 1966 – Trincardi et al., 2016, provide a full description of the
152 event). Cavaleri (2000) provides an extensive description of the original tower structure, though
153 now further improved, as the measurements on board and the derived scientific work. Firmly
154 implanted on the 16 m bottom, the three working floors of the tower are now (after the recent
155 renovation works and structural extension) respectively at 6.5, 9 and 12 m above the mean sea level.
156 The original upper part of the tower (the one up the base template) was two meter lower, and it was
157 heavily damaged during a big storm on December 22, 1979 (flood ranked #2 in Venice). Evidence
158 of high wave crests well above 9 m above the mean sea level (but with max a 1.30 m local surge)
159 was manifest. So in the recent refurbishment of the structure (after almost half a century of
160 continuous use), it was wisely decided to raise of two meters the external structure. Indeed the 29
161 October, 2018 storm was, at least for waves, an almost carbon copy of the 1979 one, and indeed

162 waves have reached again the +9 m level (again with 1.30 m surge). However, contrarily to 1979,
163 this time all the instruments worked correctly, and we now have a unique set of data for a very
164 special storm. Most of the onboard instruments are managed by ISMAR, but the tower also hosts
165 instruments by other institutions, in particular CPSM (the tidal forecast center of the Municipality
166 of Venice) and Thetis, a local environmental enterprise.



167
168 Figure 3 – Left panel: geometry of the area at the top of the Adriatic Sea (see Figure 1). The ‘tower’
169 is the position of the offshore structure shown in the right panel. Lido, Malamocco and Chioggia are
170 the three inlets connecting the sea with the lagoon. The Venice dot shows Punta Salute, the official
171 tide gauge for Venice floods.

172 The data include the following relevant parameters for our present purposes:

173 Wind – 2 anemometers (ISMAR and CPSM) at 17 m height, 3 m above the tower upper floor. Data
174 (mean wind speed, gust, direction) are available at 5' interval.

175 Waves – Five different wave systems are operated on board: a) AWAC (Nortek AS) located at 16
176 m depth, 20 m east of the tower (ISMAR). The system is composed by an acoustic doppler current
177 meter (which can also work as a profiler), an acoustic surface tracker and a pressure sensor. Integral
178 parameters are available in real time, usually estimated from the current meter and the surface
179 tracker. The once in a while retrieved raw data, then suitably analyzed, offer the possibility of 1D
180 and 2D spectral estimates. The pressure sensor provides parallel wave measurements, potentially
181 less accurate, but to be used when the many bubbles in water, following heavy breaking in a storm,

182 impede a clean acoustic signal. Current meter and pressure sensor are set to sound at 2 Hz, while the
 183 surface tracker samples the water level at 4 Hz. b) A radar surface profiler (Thetis) sampling at 2
 184 Hz. Integral parameters are available in real time, 1D spectra after the once in a while raw data
 185 recovery. c) An external acoustic echosounder (CPSM) sampling the surface at 2 Hz. Only integral
 186 parameters (no raw data) are available. It worked till a certain time, then a wave (possibly a
 187 splashing) hit and bent it. In any case problems seem to appear in strong wind conditions. d) A
 188 stereo-imaging system (ISMAR) observing in the North-East direction the area close to the tower
 189 (the waves were from South-East). The system, usable only with the daylight, provides a very
 190 detailed 2D spectrum of the wavy surface (see Peureux et al., 2018; Benetazzo et al., 2018). e)
 191 Webcams showing, apart from incoming waves, one of the pillars of the tower with direct evidence
 192 of the vertical excursion of the sea surface. Both the stereo system and the webcam signals are
 193 remotely recorded and stored for later inspection and analysis. The optical flow of information, in
 194 any case available only during the day light, stopped around 14 UTC.

195 Sea level – Four instruments: a) A conventional tide gauge (CPSM) with data at 5' interval. b) A
 196 similar system handled by ISMAR. c) A digitally filtered radar system by Thetis. d) The ISMAR
 197 ADCP.

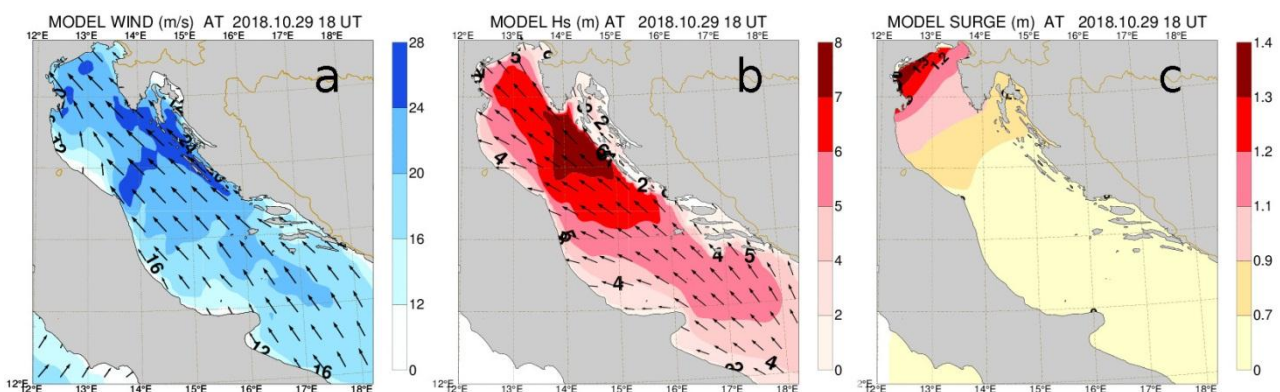
198 On the coast and the lagoon (see Figure 3, left panel) tidal data (CPSM) are available at the end of
 199 the Lido entrance jetties (2 km offshore, 6 m depth), at Malamocco and Chioggia inlets, and at
 200 several locations in the lagoon, including Punta Salute (the dot close to Venice), the official
 201 reference for Venice floods.

202

203 4 – Wind, wave and surge modeling

204 We deal with the meteorological, wave and surge aspects of the storm, the two last ones focused on
 205 the Adriatic Sea. We describe briefly the models we used. For a better understanding of the
 206 situation, we anticipate a short description of the local dominant characteristics and weather
 207 patterns.

208



209

210 Figure 4 – a) wind, b) wave, c) surge fields in the Adriatic Sea at 18 UTC of 29 October 2018.
 211 Scales are respectively ms^{-1} , m, m.

212 4.1 – Characterization of the area

213 The Adriatic Sea (see Figure 1 and the later Figure 4) is a long and narrow basin bordered by
214 mountains on both its sides. It is characterized, especially in its upper part, and in particular its
215 northern one, by two dominant winds: bora and sirocco. Bora, blowing from North-East
216 (henceforth, given their frequent use, we will indicate the four cardinal points as N-E-S-W, with
217 obvious meaning), can be very strong, but, because of fetch limitations, the derived wave conditions
218 cannot be very large. The opposite is true for sirocco, the S-E wind typically responsible for the
219 Venice floods. Warmer and humid, it is often associated to a low pressure center on the Western
220 Mediterranean basin. Sometimes, also blocked by the Alps range (see Figure 1), in the northern part
221 of the basin the wind mixes with easterly coming air leading to the so called “bora scura”, because
222 of the associated cloudy and rainy conditions.

223 The astronomical tide in the Northern Adriatic Sea, in front of Venice (see Figure 3), has about one
224 meter spring overall excursion. When the basin is perturbed by a meteorological event, two seiches
225 dominate the situation: a 11 hour one pivoting at the basin center, and a 22 hour one pivoting
226 around the Otranto strait at the southern end of the basin (Bajo et al., 2019). The bathymetry is
227 progressively shallowing towards the Venice upper end (see Figure 1). Together with the dominant
228 weather patterns, this leads to frequent and comparably large surges on its northern border, i.e. in
229 front of Venice. See Figure 4, panel c, for a clear illustration of this distribution. As shown in Figure
230 3, Venice sits at the center of a costal, 50 x 10 km wide, mostly shallow lagoon connected to the sea
231 via three inlets.

232 As a further specifications, all our times frequently mentioned are UTC that will therefore be
233 omitted. Similarly, when referring to the last days of October 2018, only the day (e.g., 29 for 29
234 October 2018) will be specified.

235 4.2 – Meteorology

236 In this study we rely on the meteorological data produced by the European Centre for Medium-
237 Range Weather Forecasts operational model (ECMWF, Reading, U.K.). The Centre runs a fully
238 coupled atmosphere-wave-ocean system. Full details are available at ECMWF IFS documentation
239 ([https://www.ecmwf.int/en/forecasts/documentation-and-support/changes-ecmwf-model/ifs-](https://www.ecmwf.int/en/forecasts/documentation-and-support/changes-ecmwf-model/ifs-documentation)
240 [documentation](https://www.ecmwf.int/en/forecasts/documentation-and-support/changes-ecmwf-model/ifs-documentation)). Presently the Tco1279 (HRES) atmospheric model has approximately 9 km
241 resolution and 137 vertical levels of which 20 are below 1000 meters. Ensemble forecasts are also
242 produced with 50 parallel runs at 18 km resolution. The operational analyses are based on 4-
243 dimensional variational data assimilation (Rabier et al., 2007), which takes operations into account
244 in a 6-hour window. The analysis data are available at 6 hour interval (00, 06, 12, 18). Being this
245 time resolution unsuitable for our purpose (in practice everything happened in 12 hours), we are
246 concatenating the first 12-hour short-term forecast fields, available at one hour interval twice a day
247 at 00 and 12. For the analysis of the event we used the +1 - +12 hr forecast fields issued twice a day
248 at 00 and 12. To explore its predictability, we have used the medium-range forecast for the 29
249 October starting up to ten days earlier, fifteen for wind gusts. Although our evaluation is based on
250 several vertical levels to obtain a general view of the overall situation, for our analysis in this paper
251 we present the surface maps that best illustrate the particularity of the conditions on the Adriatic
252 Sea.

253 4.3 – Waves

254 For wave modeling we used the WAM model, amply described in the literature; see the classical
255 Komen et al. (1994) and the ECWAM: IFS documentation CY45R1, part VII at
256 [https://www.ecmwf.int/en/forecasts/documentation-and-support/changes-ecmwf-model/ifs-](https://www.ecmwf.int/en/forecasts/documentation-and-support/changes-ecmwf-model/ifs-documentation)
257 [documentation](https://www.ecmwf.int/en/forecasts/documentation-and-support/changes-ecmwf-model/ifs-documentation) for a more specific reference to the details of its use at ECMWF. Performance is
258 available at [https://www.ecmwf.int/en/elibrary/18746-evaluation-ecmwf-forecasts-including-2018-](https://www.ecmwf.int/en/elibrary/18746-evaluation-ecmwf-forecasts-including-2018-upgrade)
259 [upgrade](https://www.ecmwf.int/en/elibrary/18746-evaluation-ecmwf-forecasts-including-2018-upgrade). Aiming at a higher resolution than the 14 km available from the Centre global model, for
260 the Adriatic Sea, as regularly done for the local operational activity (Bertotti et al, 2011), WAM
261 was run with 1/12° resolution and suitably corrected ECMWF wind speeds (more on this in the next
262 section). Full fields, and in particular the data at the ISMAR oceanographic tower, have been made
263 available at hourly intervals. 2D spectra are saved at a specified number of points, including of
264 course the tower.

265 Following the Janssen (1991) approach and the related further developments in the above cited
266 reference, the ECMWF fully coupled forecast system implies a continuous exchange of information
267 among atmosphere, wave and ocean. This is clearly not the case when running our Adriatic wave
268 model. However, with very good approximation this is not relevant because the ECMWF wind we
269 used, albeit with slightly lower wave heights, has already absorbed the interaction information.

270 4.4 – Tide and surge

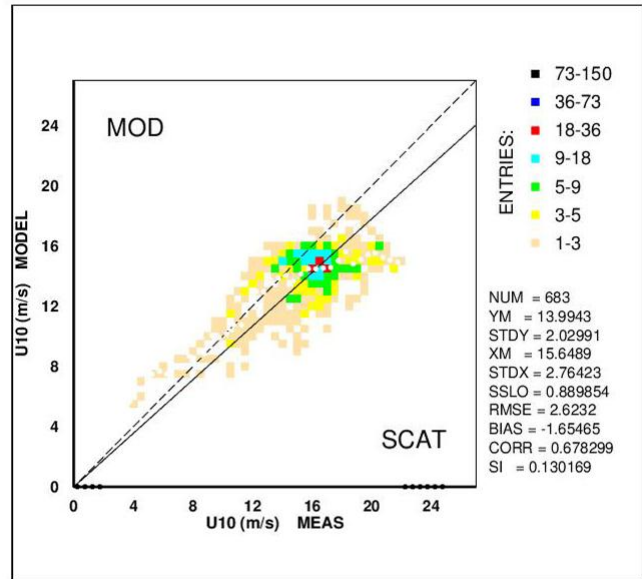
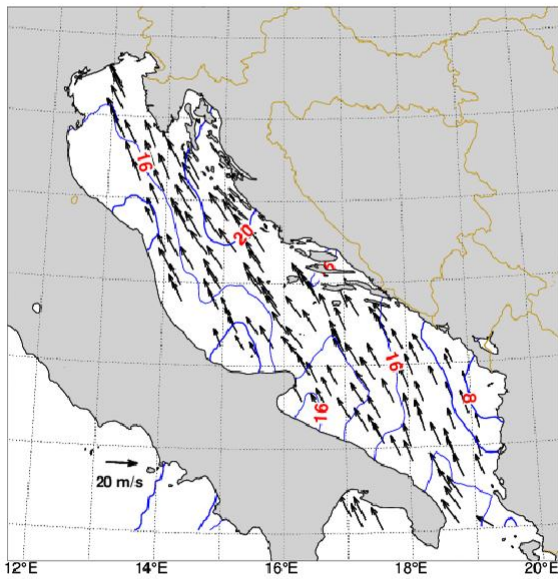
271 Sea level forecast for Venice implies modeling both the sea and the lagoon. Granted the
272 astronomical component, the storm surge contribution is evaluated with the SHYFEM model
273 (Umgiesser et al., 2014) over a spatial domain covering the Mediterranean Sea. SHYFEM solves
274 the 3D primitive equations vertically integrated over multiple z-layers and horizontally over an
275 unstructured grid. Sea level boundary conditions at Gibraltar are provided by the IBI forecast
276 system (Sotillo et al., 2015). The model has been run with ECMWF surface wind stress and
277 atmospheric pressure fields. As for waves, but more to take the white-capping input to current into
278 account, the full wind stress to the ocean has been taken into account (see ECMWF, 2018).

279 Not part of this paper, but relevant for the final discussion on the reliability of the sea level forecast
280 in Venice, using the corresponding marine conditions SHYFEM is extended to cover also the
281 lagoon (Ferrarin et al., 2010, 2013), mostly shallow (one meter average depth), but with a network
282 of deeper canals (Madricardo et al., 2018).

283

284 **5 – Modeling results.**

285 Figure 4 provides the wind, wave and surge fields in the Adriatic at 18 of 29. We use this time
286 instead of 19 (peak conditions) because, as soon explained, the meteorological model anticipates at
287 between 18 and 19 the passage of the cold front, which affects all the marine fields.



288

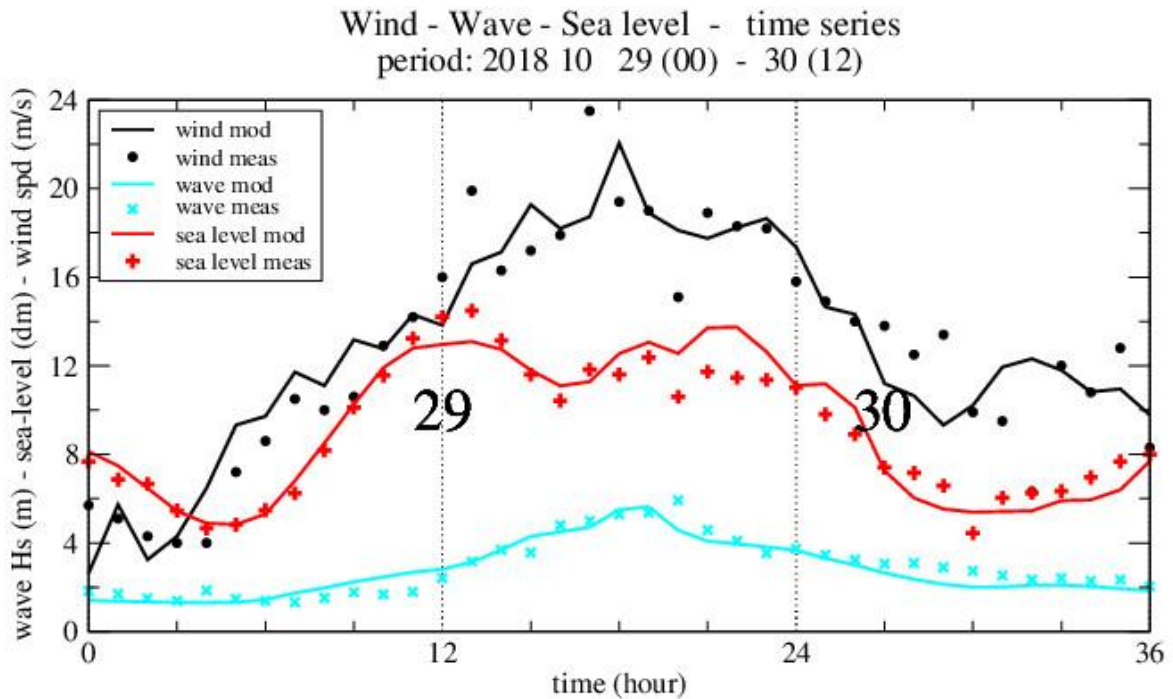
289 Figure 5 – left panel: ASCAT-B scatterometer data in the Adriatic Sea at 19.10 UTC 29 October
 290 2018. Only part of the data is shown for better visibility. The right panel shows the best-fit between
 291 ECMWF 10 m wind speeds and the ASCAT-B data.

292

293 5.1 – Wind

294 The wind evaluation is based on ECMWF operational forecasts. These wind speeds are generally
 295 underestimated in the Adriatic Sea. In general, the fields have too low speeds for the first up to 100-
 296 200 km when the wind passes from land to sea. Cavaleri and Bertotti (2004) and Signell et al.
 297 (2005) provide clear evidence of the problem in general. Incidentally, we point out this is not
 298 typical of only the ECMWF wind fields (Andy Brown, personal communication). Because the
 299 problem is permanent and repetitive, a correction is possible when used for local operational
 300 applications (see the previous section). Being fetch dependent, the underestimation, and the
 301 consequent correction, vary with the wind direction, in practice if across or along the Adriatic main
 302 axis. For the present Tco1279 resolution, 9 km, a 1.16 average enhancement is normally used for
 303 ISMAR operational activity, expected slightly in excess for sirocco, in defect for bora. However, for
 304 this specific devoted study we wished a more precise figure. Two facts helped in this respect: 1) the
 305 29 October storm in the Adriatic Sea, short and strong, was uniform in its pattern, basically a steady
 306 unidirectional sirocco wind (see Figure 4a) blowing from South-East to North-West, 2) the pass of
 307 the ASCAT-B satellite borne scatterometer all along the basin at 19.10 providing a perfect check of
 308 the model data (see Figure 5, left panel). The resulting fit is on the right one, suggesting a 1.11
 309 correction factor for the ECMWF wind speeds. This is fully consistent with previous experience. As
 310 for direction, the model wind is on average directed 2° clockwise with respect to the scatterometer
 311 data. Further, although at a point, verification in this respect has been achieved with the comparison
 312 of the data recorded at the oceanographic tower (see Figures 1 and 3 for its position). Henceforth, as
 313 in the comparison in Figure 6, our official ECMWF wind speeds will be 1.11 times the original
 314 product. We stress that 1) this is a self-standing correction, independent of the wave and surge

315 model results, 2) it is valid for this, possible for all the, sirocco storm(s) in the Adriatic Sea.
316 Different corrections may be required in other coastal areas, depending on the local geometry.



317

318 Figure 6 – Comparison between wind speeds, significant wave heights and sea levels measured at
319 the tower (see Figure 3) and the corresponding model data. Time (hours) goes from 00 UTC of 29
320 till 12 UTC of 30 October 2018.

321

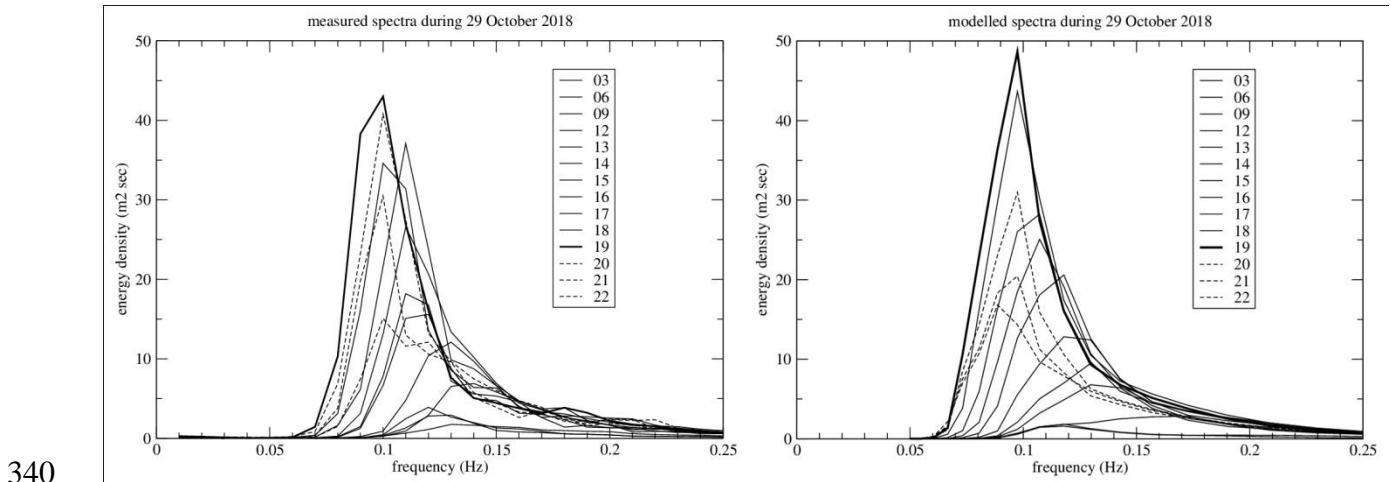
322 Figure 6 displays the evolution of the storm at the tower, starting in early 29, ending at 12 of the 30.
323 The strong dynamics of the storm, especially in its growing stage, is reflected into the irregular
324 growth of the model wind at the tower and, at a greater extent, on the corresponding recorded data
325 (hourly averages on 10' windows in the figure). We point out that the wind data at the tower have
326 not been corrected for height (taken at 17 m) and for the structure influence.

327 The instrumental wind data at the tower are available at 5' interval. This allowed to pin-point
328 between 19.15 and 19.25 the passage (see Figures 1 and 2) of the westerly violent cold front at the
329 tower. Direct inspection of the ECMWF hourly maps (forecast issued at 00 and 12) suggests that
330 already at 19 the model places the front well beyond (to the E of) the tower, in practice anticipating
331 its passing of slightly more than 30°. We will take this into account in judging the wave model
332 results.

333 5.2 – Waves

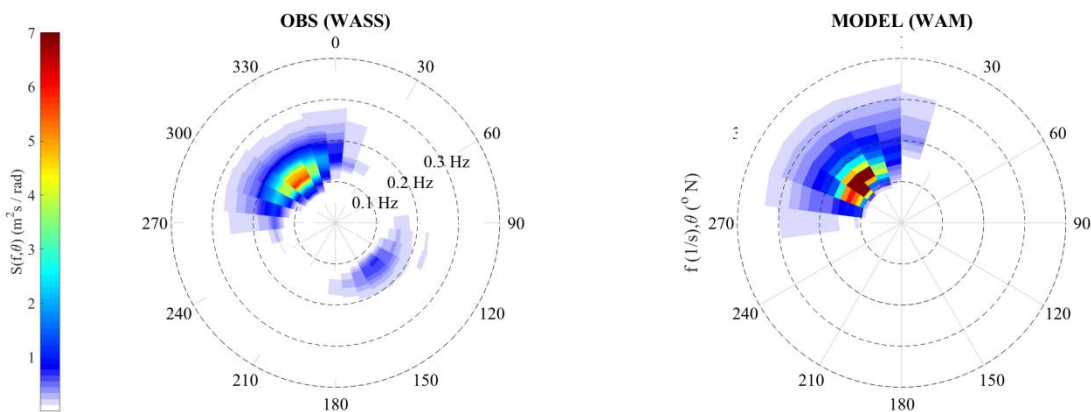
334 The wave field at 18 on 29 is shown in panel 4b. It is obviously narrowly concentrated around the
335 mean direction of the wind, the waves pounding heavily on the Venice coastline. We will describe
336 the implications in Section 7. Following both the wind distribution (4a) and the reducing depth
337 moving N, the highest waves are present on the E coast of the basin, still reaching almost 6 m

338 significant wave height H_s at the tower (see Figure 6). Following the last point in the previous sub-
 339 section, note how the model anticipates the peak of the storm.



340
 341 Figure 7 – Hourly wave spectra at the oceanographic tower. See its position in Figure 3. Left panel:
 342 measured spectra, right one: model spectra. The thin lines show the obvious growing stages of the
 343 storm. The thick line is the peak condition. The dotted lines show the progressively decreasing
 344 stages.

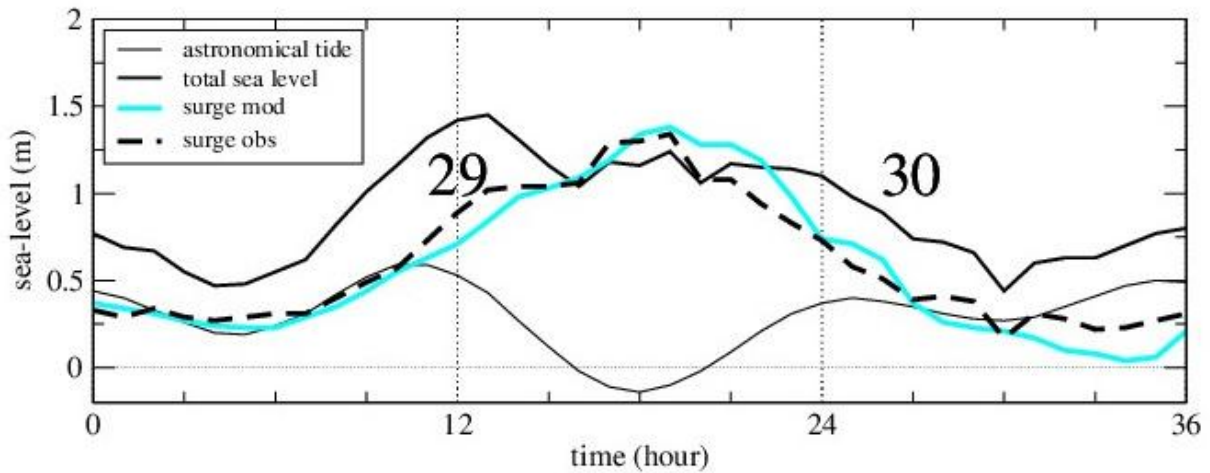
345 The measured and model spectral evolutions at the tower are in Figure 7. Referring first to
 346 measurements (left panel), we have plotted with a continuous line the growing sea conditions,
 347 marked thick the peak one, and indicated with a dash line the decreasing energy spectra. As just
 348 pointed out the peak hourly conditions are at 19. Albeit with a slightly different spectral shape, the
 349 model (right panel) provides a similar evolution. Note however the different relationship between
 350 the peak and the previous and following spectra as a consequence of the meteorological model
 351 anticipated (slightly more than 30') passage of the cold front.



352
 353 Figure 8 – 2D spectra at the oceanographic tower. See Figure 3 for its position. Left, measured
 354 spectrum (with the video stereo system); right, model spectrum. Note the opposite going waves in
 355 the measured spectrum.

356

357 As mentioned in Section 3, the stereo-video system available on the tower turned out disconnected
 358 at 14. We have so missed the initial intense part of the storm. The heaviest conditions happened in
 359 any case in the dark. However, we have a very interesting 2D spectrum at 13, shown in Figure 8,
 360 left panel the measurements, right for the model. At this stage H_s was ‘only’ 3.2 m. Granted some
 361 differences in the shape, it is clear that the two spectra are consistent to each other, as also expected
 362 from the model measurement fit in Figure 6 at this time. The remarkable not trivial detail is the
 363 patch of energy moving in opposite direction, of course in the measurements. We will come back to
 364 this in Section 7.



365

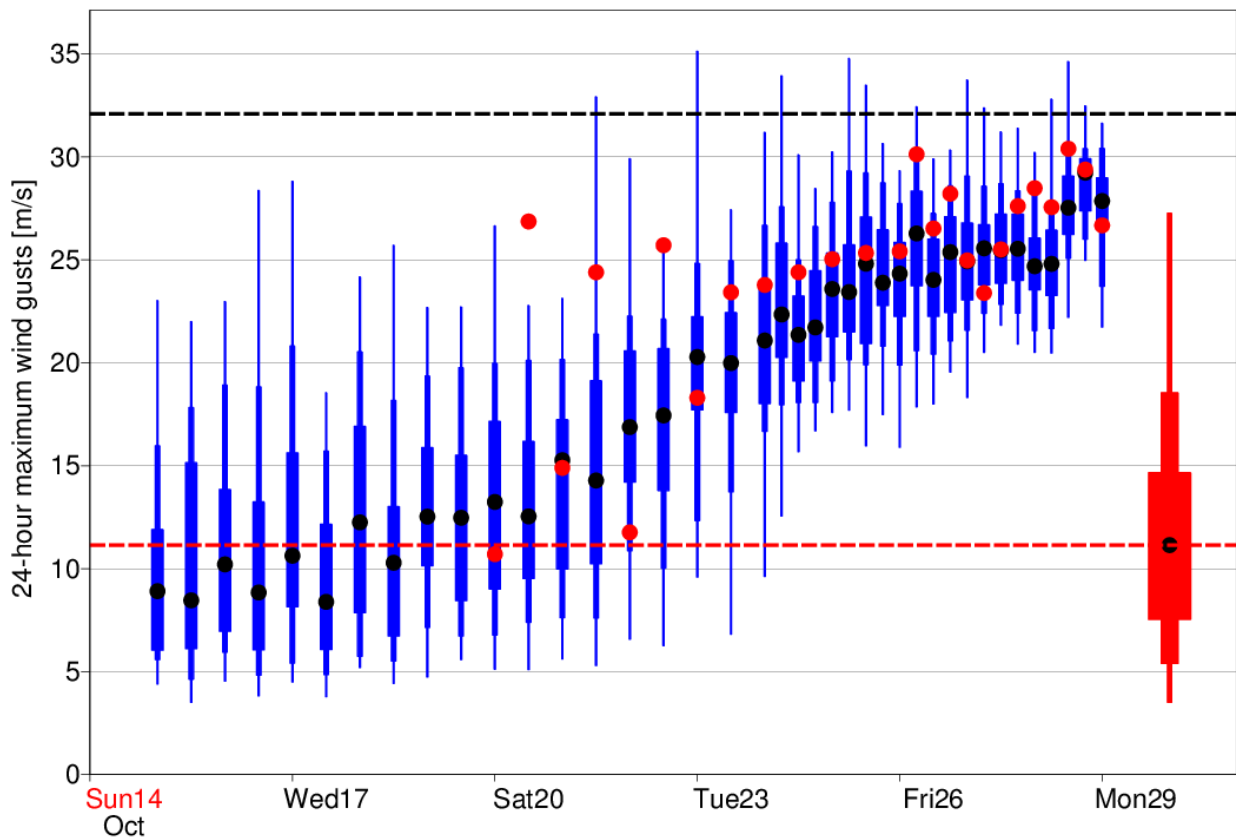
366 Figure 9 – Astronomical tide, surge and total sea level at the oceanographic tower. See Figure 3 for
 367 its position. Time (hours) goes from 00 UTC of 29 till 12 UTC of 30 October 2018. The blue line
 368 shows the modeled surge. The actual 0 of the astronomical tide is 26.3 cm above the official reference
 369 for Venice. See text for explanation.

370 5.3 – Surge

371 We have previously mentioned that geometry and bathymetry of the basin lead in stormy sirocco
 372 conditions to a strong enhancement of the surge in front of the Venice lagoon. This is evident in
 373 Figure 4c showing the situation at 18. As we will discuss in more details, there is a crucial interplay
 374 between astronomical tide and surge. While from the physical point of view we aim at estimating
 375 the non-periodic and meteo-dependent surge, the overall “tide+surge” sea level is the one of
 376 concern for coastal flooding, and in particular for the town. On this basis we compare in Figure 6
 377 the expected and measured sea level at the tower (there is a slight decrease and delay of the tide
 378 entering the lagoon – more on this in Section 7 and in the final discussion). The actual sea level
 379 peak was reached at 13, fourth historical level of flooding in Venice since 1872, start year of the
 380 measurements. Note the second sea level peak about six hours later. This point is better appreciated
 381 looking at Figure 9. This provides the astronomical tide, the overall sea level (the same as in Figure
 382 6) and (the difference) the resulting surge (dash line). Note the extent of the surge around 18, in
 383 itself 1.56 m, that only by a lucky optimal out-of-phase with the astronomical tide did not lead to
 384 the by far worst flood in history. The fourth, blue line provides the modeled surge that, with some
 385 differences along the growing and decreasing stages, managed to pinpoint time and level of the
 386 peak. Note also how the astronomical tide oscillates around a non-zero level. This is actually 26.3

387 cm (at the time of writing). The reason is historical and practical. This is the reference, at the time
 388 correct, mareographic 0 level of 1897. During this elapsed time Venice kept sinking (at different
 389 rates) and sea level rising. That mark is now 26.3 cm below the present mean sea level. However,
 390 for practical purposes the tidal information are issued with this reference, because that is what
 391 counts for the possible flooding of the different parts of the town.

392 Having acknowledged the performance of the model at short term forecast, for all practical
 393 purposes we need to assess their capability to anticipate this information. The issue of predictability
 394 is what we explore in the next section.



395
 396 Figure 10 - The box-and-whisker plot shows the evolution of forecasts for 24-hour maximum wind
 397 gusts on 29 October for the location of the tower for different starting dates. See Figures 1 and 3 for
 398 its position. The blue (red) bars indicate the 1st, 10th, 25th, 75th, 90th and 99th percentile for the
 399 ensemble forecast (model climate of the ensemble), and the red dot the HRES forecast. The black
 400 dots are the mean of the respective distributions. The 32 ms^{-1} dashed line is the peak gust recorded
 401 at the tower.

402

403 6 – Predictability

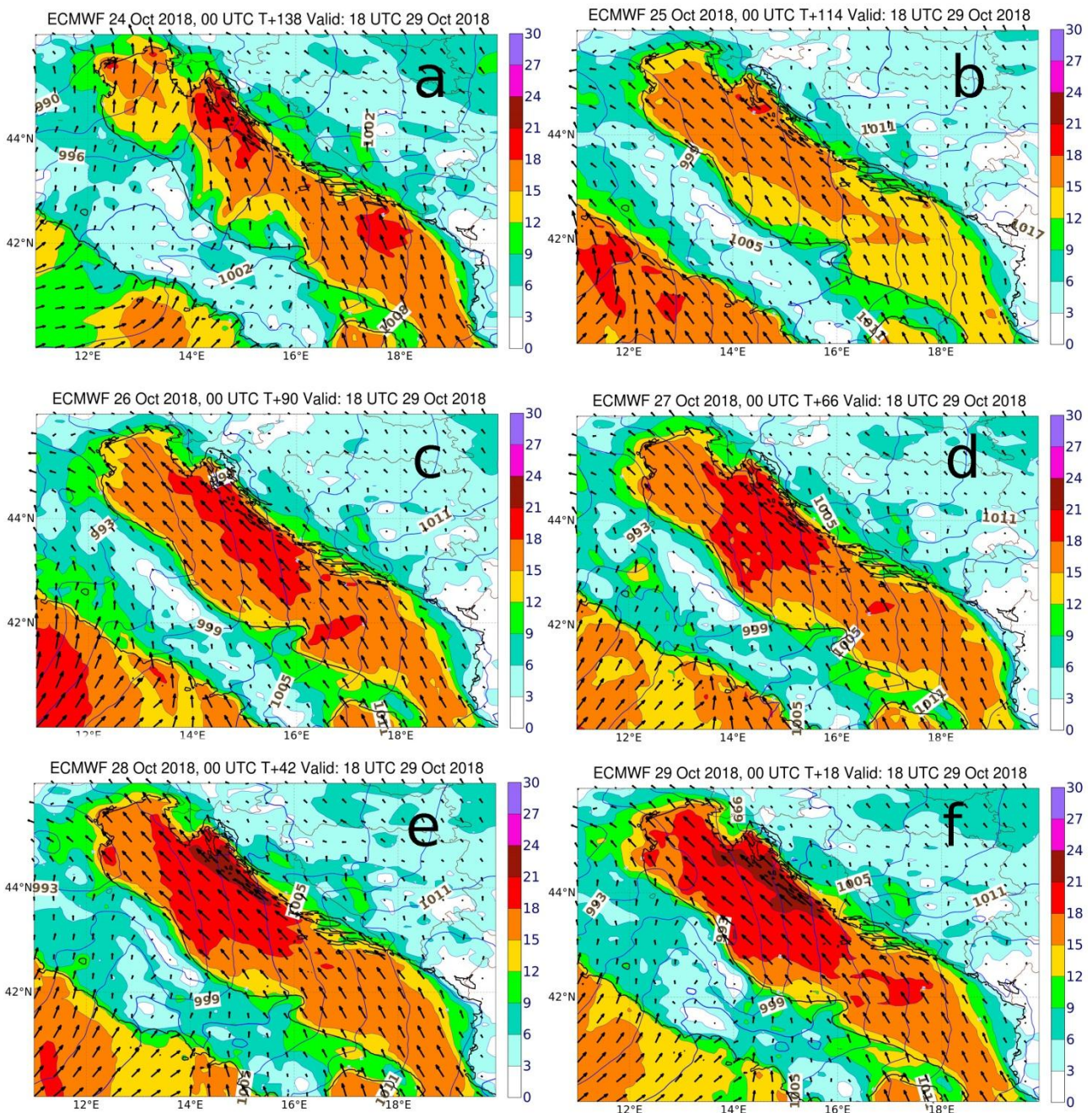
404 The purpose of this section is to assess the capability of the “ECMWF wind + WAM wave +
 405 SHYFEM surge” system to correctly forecast the events, in particular the conditions of the 29

406 October storm. This is done with two separate approaches. First, we focus on the model data at the
407 ‘Acqua Alta’ tower (see Figure 3) and verify how well ECMWF was able to forecast the local wind
408 conditions. To summarize the wind predictability of the case, Figure 10 shows a summary of all
409 high resolution (HRES) and ensemble forecasts from ECMWF for 24-hour maximum wind gusts
410 valid on the 29 and for the location of the tower. The figure also includes the model climatology for
411 the same location and time of the year. In the last forecast before the event the ensemble median
412 was similar to the 99th percentile of the model climate. For the longest forecasts included in the
413 figure (starting from 15 days before the event), the distribution of the ensemble was slightly shifted
414 to weaker gusts than in the model climate, but from eight days before the event (21 October) the
415 distribution started to shift towards higher values. From 23 October and onwards all ensemble
416 medians as well as all HRES forecasts predicted gusts above the 75th percentile of the model
417 climate. Note that the maximum recorded wind speed at the tower (1’ average) was 24.8 ms^{-1} with
418 gusts up to 32.1 ms^{-1} . It is clear that a substantial warning in this respect was available since six or
419 seven days before the event.

420 For the second approach we take a more integral view, with a look at the general fields and the
421 related integrated oceanographic results: wave height and surge. Along this line we have issued
422 medium-range (up to several days) oceanographic forecasts starting at different days/times before
423 the event, and checking the results versus the last (a few hours) forecast and the measured data. We
424 have up to ten day forecasts, using both the 00 and 12 ECMWF model runs. The time interval of
425 which the ECMWF forecast fields are stored varies with the lead time: 1 hr from 1 to 90 hr forecast,
426 3 hr from 93 till 144, afterwards 6 hr. We have interpolated in time these fields to have available for
427 each starting time a full forecast sequence of 241 (0 to 240) hourly fields. While this did not imply
428 any particular problem for waves (the Adriatic Sea wave memory is typically two days), simulating
429 surges requires a larger perspective. Indeed, for the correct evaluation of all the non-astronomical
430 oscillations in the Mediterranean, hence via the Otranto Strait in the Adriatic, typically at least a
431 month is required (Ferrarin et al., 2013). Therefore the surge model was initialized with a one
432 month simulation using ECMWF analysis data, then shifting at the day of interest to the specific
433 forecast fields.

434 An immediate perception of the general meteorological predictability is provided in Figure 11
435 showing, for the Adriatic area, the wind forecasts valid for the 29 and issued respectively at 00 of
436 24, 25, 26, 27, 28, 29. Note that for each forecast we report the conditions at 18 of 29 October.
437 While for this range of forecast the 18 fields are all close to the worst conditions, hence the fields in
438 Figure 11 are representative of the forecast situation, this is not necessarily the case for earlier
439 forecasts. This is crucial for sea level warnings, as mentioned in the previous 5.3 sub-section and
440 we will further elaborate in the final discussion. The combined information, error in range and time,
441 is provided in Figure 12. We consider the recorded maximum surge and H_s at the tower,
442 respectively 1.46 and 5.92 m, and show how the corresponding forecasts progressively approach the
443 measured values. The errors in time are provided by the horizontal bars. We see that up to five (six
444 for the surge) days earlier there were indications of a severe event, with potential warning up to
445 eight days forecast range. As Grazzini (2007) and Cavaleri et al (2010) discuss for the other two,
446 1966 and 1979, historical cases, an extended predictability seems to be a characteristic of these
447 strong events that, on a more general perspective and as described in Section 2, follow a well-

448 defined meteorological pattern typical of the Western Mediterranean basin in the Fall. More on this
449 in the final discussion.

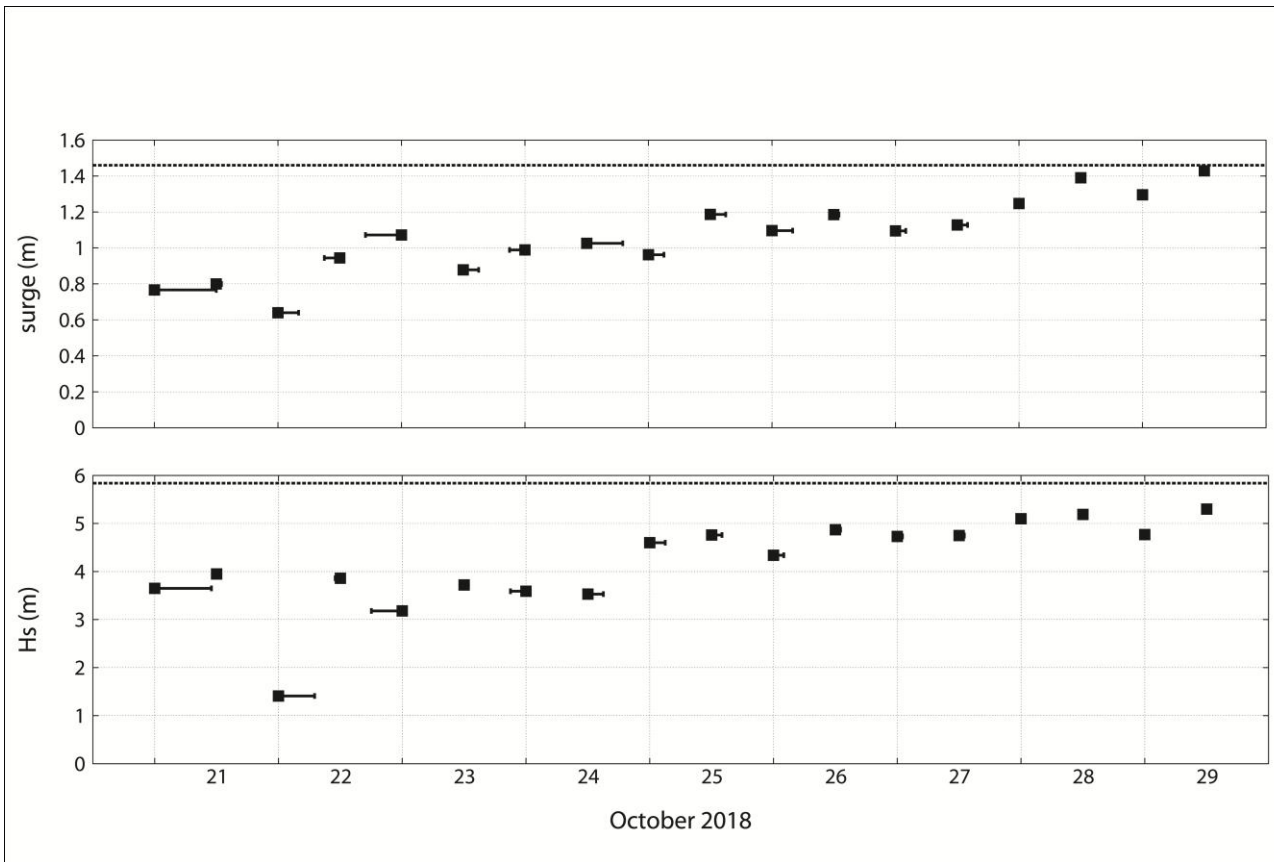


450
451 Figure 11 – Adriatic Sea. See Figure 1 for its position. Wind fields at 18 UTC 29 October 2018
452 according to the forecasts issued respectively at 00 UTC of a) 24, b) 25, c) 26, d) 27, e) 28, f) 29
453 October 2018.

454
455 **7 – Coastal physics**

456 Till now we have focused our attention on the whole Adriatic Sea, checking at the tower, 15 km
457 offshore, our modeling results. It is time to zoom more on the area shown in Figure 3, exploring the

458 consequences of a strong storm on the coastal environment. We touch in sequence four subjects:
 459 coastal set-up, modeling the sea level in the lagoon, the passage of the front, the implications of the
 460 opposite going waves in Figure 8.



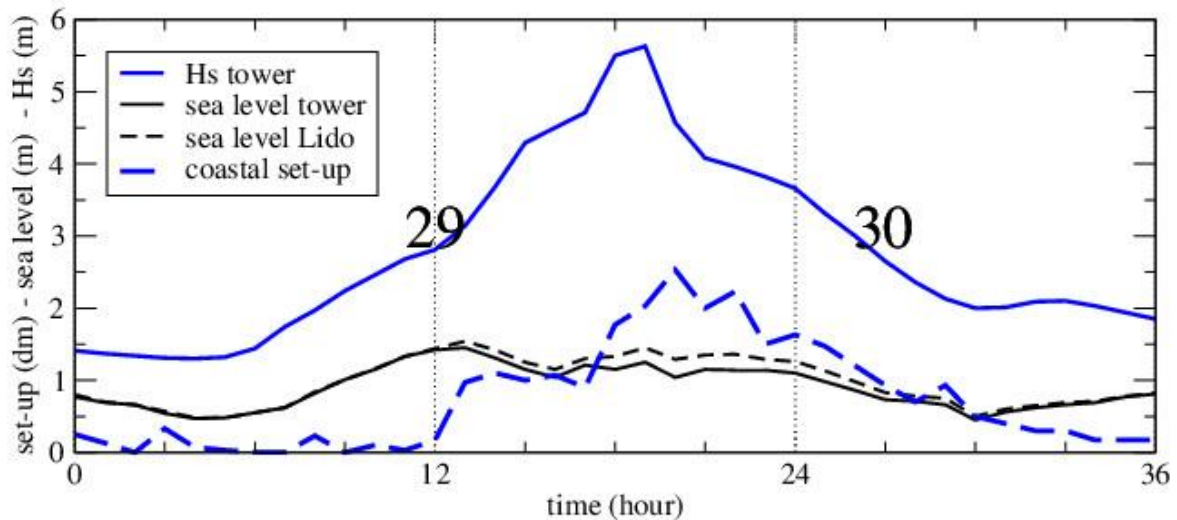
461
 462 Figure 12 - Predictability of the 29 October 2018 event. The two panels show the corresponding
 463 surge and significant wave height forecasts issued at different dates and time. The horizontal bars
 464 show the errors in timing the worst 29 October 19 UTC conditions. The two horizontal dashed lines
 465 show the respective measured values.

466
 467 7.1 – Coastal set-up

468 The storm of 22 December 1979 destroyed part of the over-structures of the tower (they were two
 469 meters lower than now), including the onboard energy supply system. Only two records survived
 470 thanks to mechanical recording: wind and sea level. The latter, first assumed to be wrong because of
 471 the sea conditions, turned out to be the first solid evidence (coastal-offshore sea level) of wave set-
 472 up (Longuet-Higgins and Stewart, 1964, Bowen et al., 1968). See Bertotti and Cavaleri (1985) for a
 473 full description of the data and related modeling.

474 The 1979 and 2018 storms were of comparable intensity, H_s in particular. Hence a similar effect is
 475 to be expected for the last year storm. This is clearly shown in Figure 13 where we plot the sea level
 476 recorded at the tower and at the coastal tide gauge located (Figure 3) two km offshore, at the end of
 477 the Lido jetty. The relationship between the wave heights at the tower and the ‘Lido – tower’ sea

478 level difference is evident. However, this is only part of the story. As we will soon discuss in sub-



479

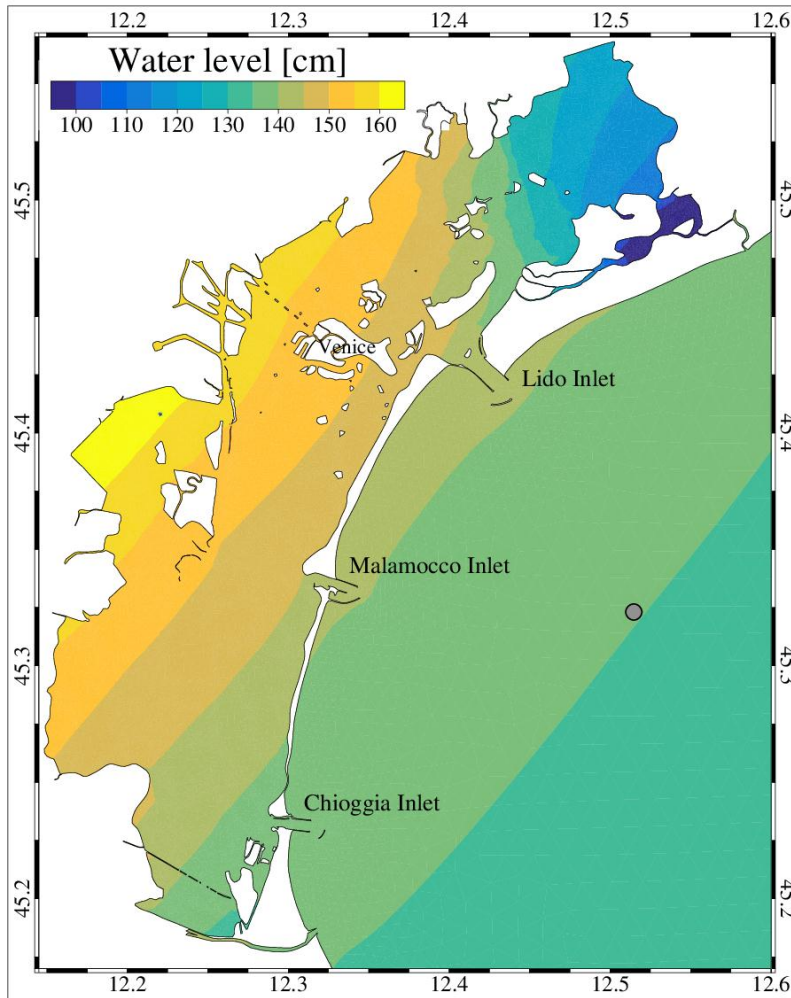
480 Figure 13 – Sea level at the coast (Lido inlet) and the tower. See Figure 3 for their position. The
481 other two lines show the respective difference (coastal set-up) and the significant wave height at the
482 tower. Time (hours) goes from 00 UTC of 29 till 12 UTC of 30 October 2018.

483 section 7.3, wind has a role as well. In equilibrium conditions a surface wind stress towards the
484 coast must correspond to a sea level gradient in the same direction. This is inversely proportional to
485 the local depth, hence quickly growing approaching the shallower coastal waters. Therefore part of
486 the cited ‘coast-tower’ sea level difference is due to wind as well. However, wind practically
487 stopped at the end of the day, while swell kept pounding on the coast, hence the parallel decrease
488 also on the 30 of the wave height and the coastal set-up.

489 Two more things need to be pointed out. First, the sea level at the Lido jetty is the one of relevance
490 for Venice, forcing the input to the lagoon. Second, given the depth at the jetty end, a much higher
491 set-up was present at the coast, as documented by the reported extended damages.

492 7.2 – Modeling the sea level in the lagoon

493 As described in subsection 4.3, the SHYFEM model is extended to the lagoon modeling the related
494 sea level distribution. The mostly shallow (1 m) water of the lagoon makes the surge distribution
495 very sensitive to wind. This is clearly shown in Figure 14 where we show the modeled water level
496 distribution in the coastal and lagoon areas. Knowing the wind direction, from S-E to N-W, it is
497 immediate to recognize the dominant effect of the wind, better said, of the local wind stress, on the
498 overall level distribution. Both in the sea and the lagoon the isolines are practically perpendicular to
499 the wind direction. An exception is the northern area of the lagoon where the hysteresis of the
500 system, with the implied delays, dampens the higher oscillations present on the other parts of the
501 lagoon.



502

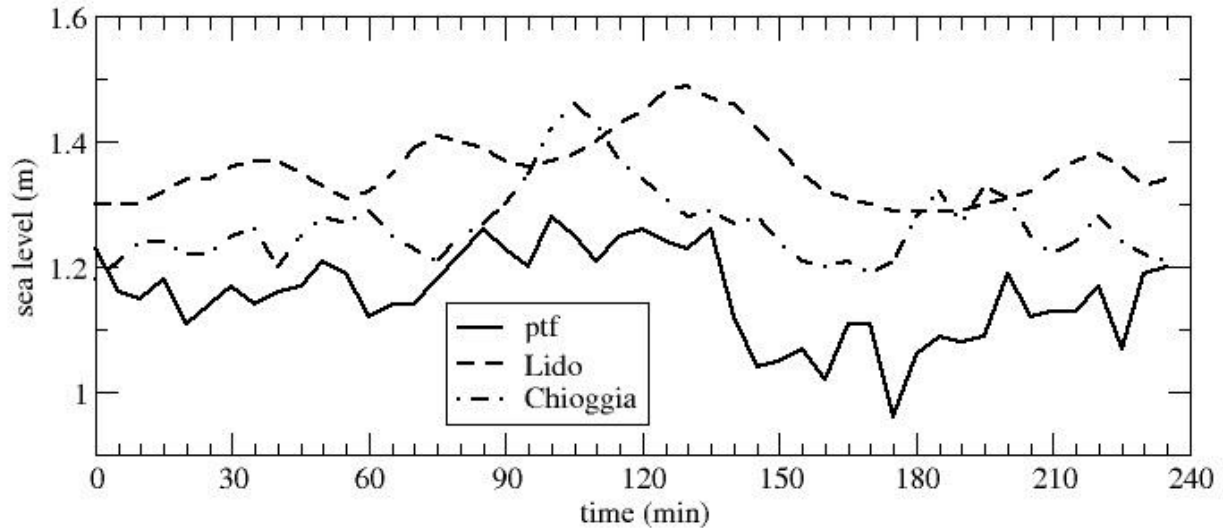
503 Figure 14 – Modeled sea level distribution at 18 UTC 29 October 2018 in the area off the Venice
 504 coastline and in the lagoon. See Figures 1 and 3 for their position. The small circle shows the tower
 505 position.

506 7.3 – Front passage

507 In Section 2, describing the evolution of the meteorological situation on northern Italy, we have
 508 mentioned how after 18 an energetic cold front crossed the Apennines and advanced over the
 509 Northern Adriatic Sea. Indeed, after several hours of continuous sirocco, the wind record at the
 510 tower, at 5' interval, documents the passage of the cold front at 19.15 (wind changes direction by
 511 40° clockwise). The tide gauges data strongly suggest that the change implied a rapid readjustment
 512 of the sea level distribution in the coastal area, including the tower.

513 Figure 15 shows the sea level, at 5' interval, recorded at the tower, the Lido gauge and at the
 514 Chioggia inlet. See Figures 3 and 14 for the local geometry. The dominant feature is the drop of sea
 515 level, more than 20 cm in 10', at the tower, happened soon after the front passage. Our
 516 interpretation is as follows. With wind blowing and wave moving perpendicularly towards the
 517 coast, there is a pile up of water at the coast (just discussed in sub-section 7.1). At any instant the
 518 “towards the coast up-slope” is supported partly by the wave set-up, partly by the local wind stress.
 519 A sudden change of wind direction changes abruptly the supporting surface stress. The system (the
 520 sea level distribution) must adapt to the new situation, the new equilibrium implying a lower up-

521 slope with a consequent rapid redistribution of the related water mass. Granted the lack of details of
522 the forcing situation, we suggest this to be a unique case where we have, in an indirect way, a
523 physical evidence of, hence the possibility to estimate, the surface stress to the ocean.



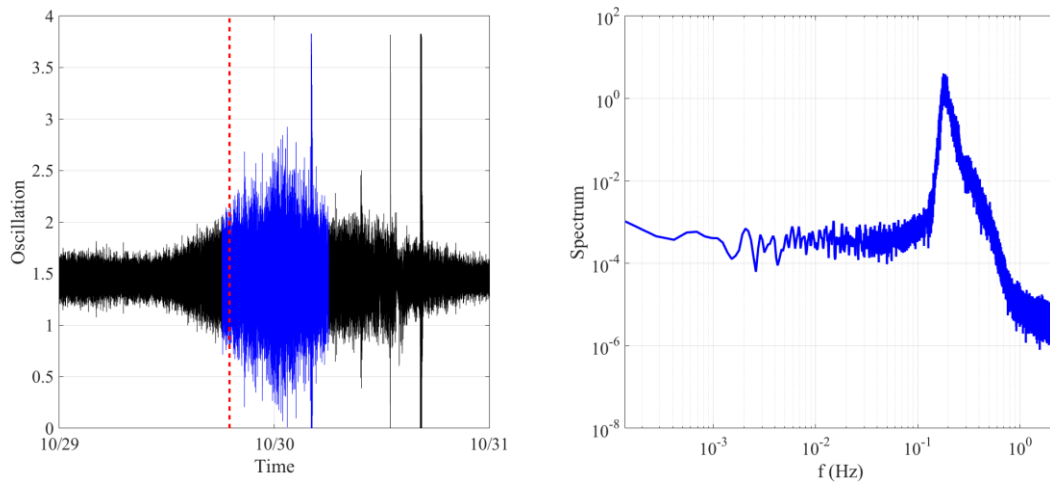
524

525 Figure 15 – Time history (17-21 UTC 29 October 2018) of the recorded sea level at the tower (ptf)
526 and Lido and Chioggia inlets. See Figure 3 for their positions.

527 Our interpretation of the front passage is supported also by the records at Lido and Chioggia inlets
528 (Figure 15). Malamocco data are not available for flooding of the gauge well in heavy sea
529 conditions. Both the Lido and Chioggia records show a rapid increase of the local sea level before
530 the rapid decrease. A possibility we suggest is that the advancing front, with wind oblique with
531 respect to the sirocco, was also pushing water in its direction. So the front was not only
532 meteorological, but also oceanographic, leading to a temporary increase of the coastal sea level
533 followed, soon after the front passage, by an even more rapid decrease. That both these growths and
534 decays, at the two gauges, are associated to the front is shown by their different timings. Chioggia
535 (see Figure 14) is situated about 20 km W of the tower, Lido slightly to W. The signal at Chioggia
536 in Figure 15 appears about 25' before than at Lido, and 30' before the one at the tower. This
537 suggests a 40 km h^{-1} frontal speed, fully consistent with the general characteristics of an energetic
538 front and with data derived from the meteorological maps (but the model slightly anticipated the
539 passage of the front).

540 With a sort of sensitivity analysis we have done a crude attempt to verify if, with the available data,
541 the SHYFEM model could reproduce such a situation. Lacking a more detailed description, we have
542 simply stopped the wind input to the model at 19.15 (i.e. at the front passage) to see how the model
543 reacts to a sudden stop of the wind stress. Indeed (not shown), the model does show a more rapid
544 decrease of the sea level than in the normal situation, but the data presently available are too crude
545 in space (ECMWF model) and time (once an hour) to allow a sufficiently detailed picture of the
546 situation. We are talking of variability at the scale of kilometers and minutes with the system (the
547 local sea level distribution) reacting on the same scale. While a tentative reconstruction of the

548 forcing fields will be done in the future, we offer this as a test case to test at their limits the various
549 surge and small scale circulation models.



550

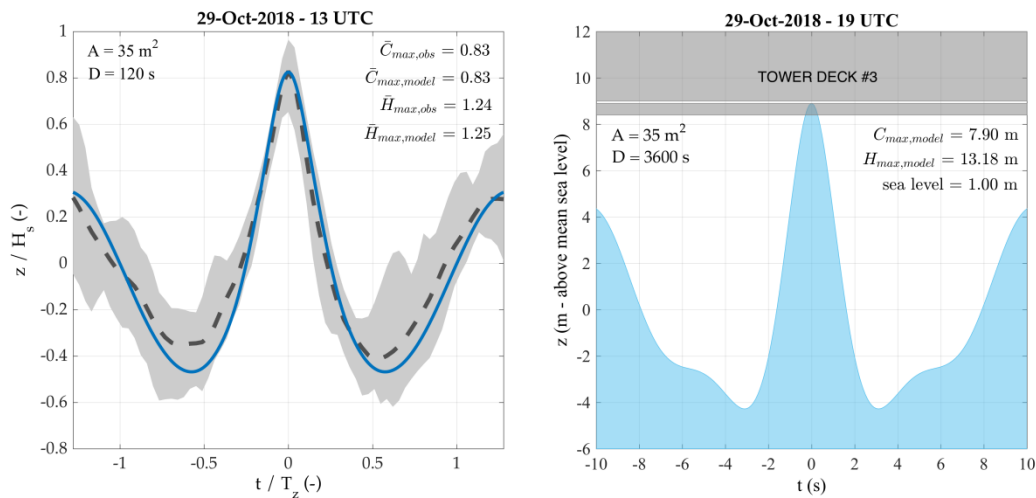
551 Figure 16 – Left panel: original output (29-30 October 2018) of the seismometer at Padua
552 University, 40 km inland with respect to the coast. To the right: spectrum at the time of the red
553 dashed line.

554 7.4 – The opposing swell

555 We have pointed out in Figure 8, looking at the very detailed 2D spectrum derived at the tower with
556 the video stereo system (although, for the specified reasons, not at the heaviest conditions), the
557 presence of wave components moving in a direction opposite to the main flow and the wind. This
558 was the first evidence in this sense, and it attracted therefore our attention. Excluding, with a bit of
559 pragmatism, any local dynamical non-linear behavior, the simplest explanation was a reflection
560 from the coast. We were a bit skeptical because the 1/1000 bottom slope toward the coast with a
561 very flat final beach does not suggest an effective reflection. However, at the same time we were
562 provided with some seismometer data from Padua University, 40 km inland. The particularly strong
563 signal of 29 and 30 is shown in the left panel of Figure 16.. It is difficult not to think of an
564 association with the contemporary storm. Inland seismometer records of offshore wave conditions,
565 if strong enough, are a known fact. Starting with the 1951 basic dissertation by Longuet-Higgins on
566 the subject, this was taken up again in recent times by Kodar et al. (2008) and Ardhuin et al. (2012),
567 among others. However, for waves approaching the coast to generate inland microseisms a certain
568 level of reflection by the coast is required. We thought this unlikely on the Venice beach. However,
569 the correct link was provided by the spectrum in Figure 8, showing beyond any doubt the presence
570 of reflected waves. We can only hypothesize that the heavy wave conditions, supported also by the
571 coastal set-up, led to different breaking on the beach, with a potential reflection enhanced by the out
572 of season sandy walls erected to protect the tourist infrastructures. The typical link between sea
573 waves and seismometer signal implies that the seismic wave has a double frequency with respect to
574 waves. The right panel of Figure 16 shows the seismometer spectrum at the peak of the storm. The
575 peak at 5 s period, half of the one of incoming waves, is unmistakable. However, we warn that 5 s is
576 also close to the natural period of the seismometer, but the much stronger signal following the
577 energy of the storm is quite clear. Not shown, in the seismometer spectra before and after the storm
578 the seismometer spectral peak is drastically lower and at a lower frequency.

580 **8 – The highest wave heights**

581 In practical applications, as e.g. the cited ECMWF forecast activity, the standard output of the wave
 582 model includes the 2D spectral distribution in space and time. Given the wave conditions at known
 583 time and location, a strong required piece of information is the height, or crest height, of the
 584 expected largest wave. See Benetazzo et al. (2017) and Cavaleri et al. (2017) for a discussion of the
 585 matter. The availability at the tower of both detailed wave measured data (stereo video system and
 586 single point radar – see Section 3) and model spectra allows a keen verification of the theoretical
 587 approach in heavy sea conditions.



588

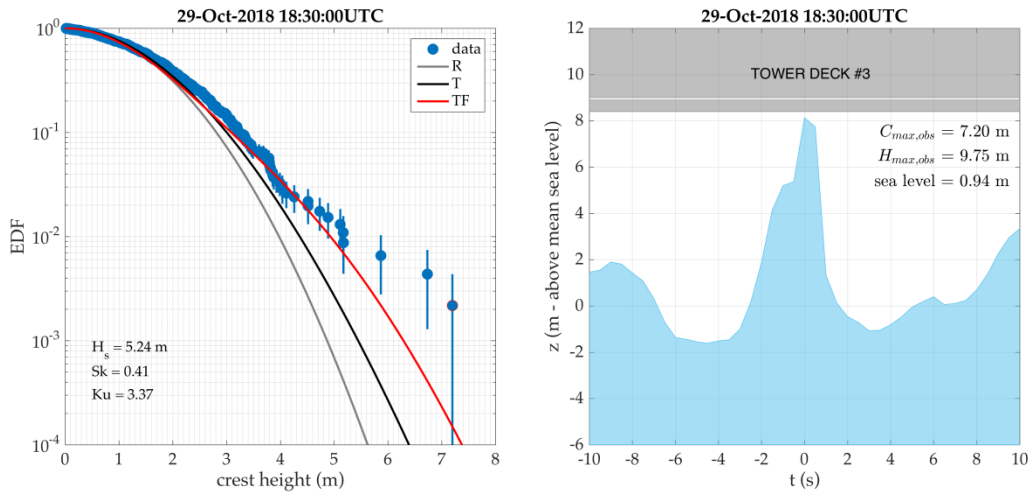
589

590 Figure 17 - Largest wave heights. Left panel: normalized profile of the expected largest wave at the
 591 tower at 13 UTC, from stereo observations (black dashed line) and model estimate (blue solid line).
 592 Space and time intervals considered are 35 m^2 and 120 s . The gray region represents the confidence
 593 limit of the observations. Right panel: profile of the wave with the largest expected crest height at
 594 19 UTC, from model estimate, compared to the highest tower deck that was damaged. Space and
 595 time intervals considered are 35 m^2 and 3600 s . Sea level at the time was 1.00 m .
 596

596

597 The left panel of Figure 17, based on the wave conditions at 13, compares the expected (blue line)
 598 maximum crest height and profile derived using the WAM model spectrum with (dashed line) the
 599 corresponding result derived from the stereo system. The shadow represents the confidence limits
 600 associated to the measurements. The considered space and time intervals are 35 m^2 and 120 s
 601 respectively. At this time the significant wave height was 3.2 m . The agreement of the observed and
 602 modeled profile allows inferring the profile of the wave with the largest expected crest height at 19,
 603 close to the heaviest conditions at the tower. This is shown in the right panel for 35 m^2 and 3600 s .
 604 The height reached by the crest of the largest expected wave (7.90 m) is compared to the height of
 605 the damaged structure suspended below the tower deck n. 2. This deck corresponds to the level of
 606 the outgoing horizontal platform (Figure 3) at the second floor of the tower. The nominal height on
 607 the mean sea level of the suspended structure is 8.40 m , reached by the wave crests during the storm

608 because of the higher sea level present at that time. This is why in the figure the waves are not
 609 waving with respect to the mean sea level, but to the one at that time (+0.94 m).



610
 611
 612 Figure 18 – Largest wave heights. Left panel: exceedance distribution function (EDF) of the
 613 observed crest heights (data, blue dots), from the single point radar (3600 s). Theoretical EDFs are
 614 plotted for reference (R: Rayleigh, T: Tayfun, TF: Tayfun-Fedele). Right panel: profile of the wave
 615 with the largest crest height, compared to the highest tower deck where damage was reported. Sea
 616 level at the time was 0.94 m.

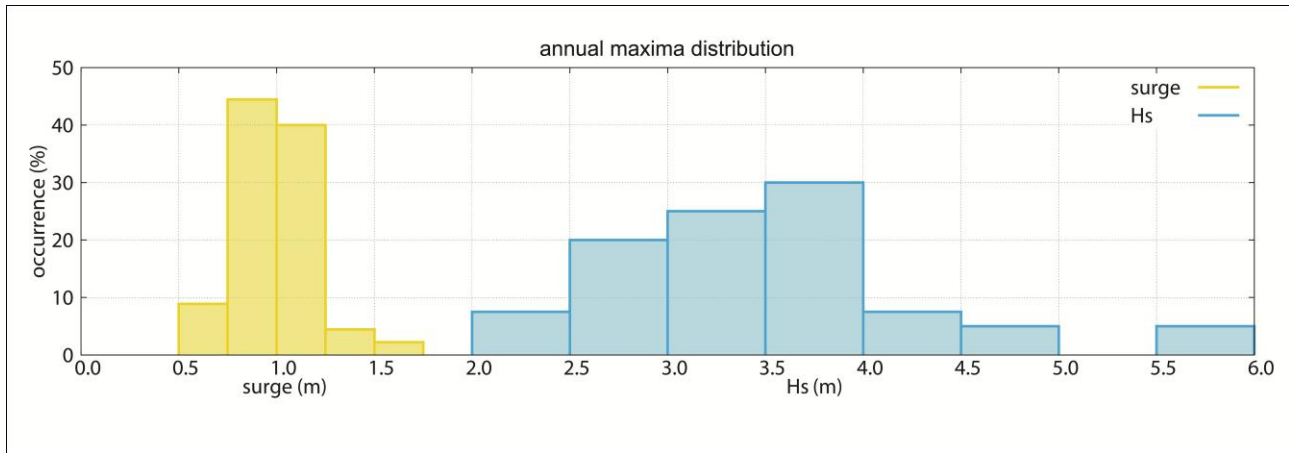
617
 618 Figure 18 provides a similar information based on the observed single point radar data available at
 619 the peak of the storm. During the 18-19 radar record (7200 data at 2 Hz) several apparently
 620 anomalous crest heights were recorded that prompted a keen verification of the record. The one in
 621 the right panel is an example. Excluding (by direct inspection) spikes and other anomalous reasons
 622 as possible explanations, we explored the related crest height distribution. The result is in the left
 623 panel. Here we have plotted three distributions, in increasing level of non-linearity of the process,
 624 respectively Rayleigh, Tayfun and Tayfun-Fedele (2007), this last one (TF) accounting for
 625 skewness and kurtosis of the sea state (0.41 and 3.37, respectively). Looking at the figure, it is
 626 obvious that the data follow well the TF distribution, but only up to a certain point, after which we
 627 find a few “anomalous” very high values. We do not have an explanation for them. We stress that
 628 the commonly used definition of “anomalous” implies in itself something exceptional, something
 629 that by instinct we tend to associate to a single (the so called freak) event. However, this is no more
 630 the case when we have three or four of them out of 360 waves. If, as it is the case, this is not due to
 631 an instrumental error, physics must be at play, a physics we do not fully understand. We will
 632 comment further on this in the last section.

633

634 9 – Long term statistics

635 When a rare, especially if damaging, event takes place, it is natural to ask how rare it was, or, in
 636 other often used words, which is its expected return time. Several attempts have been done in the far
 637 and recent past to fit the Venice surge data with some extreme distributions, and a large range of

638 different results has been obtained (Marani, personal communication). Obviously the 29 October
639 event will lead to new estimates. Rather than entering this game, we want to look at the problem
640 from a different perspective. Clearly the origin of everything is meteorological, but usually people



641

642 Figure 19 – Statistical distributions of the maxima surge η and significant wave height H_s values for
643 all the events for $\eta > 0.5$ m and $H_s > 2.0$ m. The period considered is 1979 to present.

644 pay a special attention to measured data. For our interests the two main parameters are surge level
645 and significant wave height H_s , in particular in front of Venice. Thinking to the input to the
646 corresponding models, wind and surface pressure, wave height appears as a more general parameter
647 because representative of the conditions on the whole Adriatic basin, while, as we have seen, surge
648 is highly dependent on the ones in the last tens of kilometers before the coast. In any case, surge or
649 H_s , the peculiar point we want to call the attention to is how the 1966, 1979 and 2018 cases fit in the
650 general distributions. Using, for the specified reasons, H_s as example, we consider the distribution
651 of its peak values for all the 1979 to present storms, based on the historical directional wave dataset
652 recorded at the Acqua Alta tower, as documented in Pomaro et al., 2018. We then find a regular,
653 continuous distribution up to 4.6 m, after which the void before the two isolated values 5.92 (2018)
654 and 6.0 (at least, 1979, from the hindcast and the damages to the tower). In any case a similar, more
655 quantified argument can be done for the measured surge, with 1.25 and 1.50 m (respectively for
656 1979 and 2018). The actual distributions are shown in Figure 19, where we plot the number of
657 occurrences for each wave height and surge range. Although less so for surge, it is clear that the two
658 cited storms stand by themselves, certainly so for wave heights that, as we mentioned above, are
659 more significant for the general meteorological situation. The distribution is even more singular if
660 we take into account the 1966 storm, where surge (1.66 m) and wave height (much larger than 6 m)
661 were the highest ever remembered. There were enormous damages on coastal structures. As an
662 example, the last 200 m of the six jetties at the lagoon inlets were not existent after the storm.

663 We do not have, and as far as we know no one has, an explanation, except invoking (a rather slim)
664 chance. On a completely different perspective we wonder if these storms do indeed belong to the
665 same kind, or family, of storms of the other milder events. It is clear that the problem is
666 meteorological, because this is the genesis of both surge and waves. A reason for arguing is also
667 that, apart from the 2018 explosive cyclogenesis, the three storms have almost identical genesis and
668 meteorological pattern. This is of course a point to keep in mind. We do not have the reply, but at
669 the same time we do not think that invoking only the random chance is the reply as well.

670

671 **10 – Discussion**

672 Following the large scale storm that affected Northern Italy at the end of October 2018 (large waves
673 also in the Ligurian Sea (see Figure 1) and the strong wind on the Eastern Alps), in this paper we
674 focus on the sub-events on the Adriatic Sea. The reason is that these sub-events deserve by
675 themselves a devoted attention, on one hand for the level of the storm and its implications, on the
676 other hand because the contemporary availability of both offshore and coastal data has allowed
677 specific considerations on several aspects of coastal physics. We discuss in sequence the relevant
678 aspects of our results.

679 The storm

680 In one way the storm was typical of the Fall. In this period, following the often still Summer like
681 position of the Azores anticyclone and the growing cold inputs from Northern Europe, a cold
682 tongue of relatively low pressure air protrudes from France into the Western Mediterranean basin. If
683 cold air bursts in from the Gulf of Lion (see Figure 1) on this area, the strong contrast with the still
684 warm water leads frequently to the formation of a cyclogenesis. In turn, especially if constrained by
685 a high pressure on the Balkans, this leads to strong S-E (sirocco) winds on the Adriatic Sea, hence
686 to high waves and surge in front of the Venice coast. In the present, 29 October 2018, case the
687 overall pattern was complicated, and made in itself unique, by the intensity of the explosive
688 cyclogenesis, the consequent (cited above) storms on the Ligurian Sea, the intense storm in the
689 Adriatic Sea, and the strong winds on Eastern Alps.

690 Predictability

691 Previous studies of this kind of storms, especially if very intense (see, among others, Cavaleri et al.,
692 2010), suggest a possible good level of predictability. Indeed the general meteorological pattern is
693 typical of major precipitation events in the Mediterranean in the Fall, and therefore we should
694 expect to be able to anticipate its development (Grazzini, 2007). Strong wind gusts, at the extreme
695 of the climatological distribution, were available on the forecasts up to eight and nine days ahead.
696 Our oceanographic experiments with forecasts up to ten days before the event show this is indeed
697 the case. Good quality predictions, certainly so for the overall situation, were available till five or
698 six days before the event. Its strength may have been underestimated, less so approaching the date,
699 but the warning of something special going to happen was there. Mild warnings were available till
700 eight days ahead. This, up to six days ahead as tested at the time, is consistent with the results
701 previously obtained (Cavaleri et al., 2010) for the other two similar events of 1966 and 1979.
702 However, this is much less the case for the explosive cyclogenesis we have seen in Figure 2b and
703 described in Section 2.

704 Modeling

705 The wind fields on the Adriatic Sea are strictly associated to the overall meteorological structure. In
706 the present case we were fortunate to have the pass of a scatterometer at the peak of the storm, with
707 a consequent direct verification of the model surface wind field. This confirmed what already
708 known and regularly considered in our Adriatic operational activity: the ECMWF wind fields are

709 locally geometrically correct, but slightly underestimated as wind speed is concerned. This is a
710 known problem with offshore blowing winds, hence relevant in enclosed seas and coastal
711 environments, notably present also (personal communication) in the UKMO and NCEP surface
712 products. This is regularly taken into account in our local operational activity, but the passage of
713 ASCAT-B allowed a more specific correction. We stress again this is uniquely a wind correction,
714 based on objective data, independently of the following wave and surge results. With the correct
715 wind these were very close to the respective measured data, slightly less so for the significant wave
716 height, the difference possibly related also to the confidence limits of the measurements.

717 Timing of the cold front

718 The development of the general meteorological pattern is well forecast by the meteorological
719 model. This is less the case for what concerns the strong cold front. Indeed it is not easy to pinpoint
720 the correct dynamics of these very strong mesoscale events. This is true in particular for their
721 translation speed. The high frequency (5') data at the tower clearly show that the model anticipates
722 the passage of the front by more than half an hour, with a consequent positional error of 30 or more
723 kilometers. This is clearly seen comparing the 19 and 20 maps (not shown) versus the tower and
724 coastal wind and tidal data. This time shift needs to be taken into account when comparing general
725 model and measured data.

726 Surge

727 The map in Figure 4c and the coastal set-up in Figure 13 show very clearly how the surge is
728 concentrated (under sirocco conditions) on the last tens of kilometers before the Venice coast. The
729 consequent strong spatial gradients hint to the difficulty of identifying the correct surge for the
730 estimate of the possible Venice flood. The relevant value is not the one at the coast, but the one two
731 kilometers offshore, at the sea exit of the jetties bordering the inlets to the lagoon. Two things need
732 to be pointed out. First, the set-up at the coast is consequently much larger than the one at Lido
733 shown in Figure 13. Second, the lagoon has then its dynamics that, only hinted to, but not dealt
734 with, in this paper, needs to be properly modeled.

735 Flooding in Venice

736 The actual sea level, in town as everywhere else, is the addition of the just mentioned surge and the
737 regular astronomical tide. We stress the crucial point of the relative timing between the two
738 components. As mentioned in sub-section 5.3, on October 29 we were very lucky because the two
739 components were 90° out of phase, and indeed the flood peak happened with only less than half a
740 meter surge contribution. Had the 1.54 m surge happened a few hours before, conditions would
741 have been disastrous.

742 This takes us to the subject of sea level predictability. As stressed at the first two items of this
743 section, we can rely on a sufficient level of predictability for what concerns the strength of the
744 storm, but timing is another matter (see in this respect Figure 12). At three or four day forecast
745 horizon an error of a few hours (out of 72 or 96) is considered negligible for most practical aspects.
746 However, such an error may have dramatic impacts on the expected overall sea level because of

747 surge timing with respect to the astronomical component. There is no way out. The only solution is
748 to work with ensemble forecasts, providing the statistical distribution of the combined possibilities.

749 Offshore and coastal data

750 The availability of measured data at the offshore tower and at the coast has made evident the
751 relevance of the physics of coastal processes for local modeling. The substantial sea level
752 differences between the 15 km distant locations are to be associated to 1) the wave set-up due to the
753 progressive bottom induced breaking moving to shallower and shallower waters while approaching
754 the coast, 2) to the surface up-slope towards the coast associated to the surface wind stress acting on
755 relatively limited depths. In particular the passage of the cold front has made evident, via the quick
756 collapse of the sea level at the coast and in particular at the tower, the role of wind stress in keeping
757 the water towards the coast. Having, although without all the necessary details, the wind fields
758 before and at the passage of the front, in principle we should be able to derive the actual wind
759 stress, a notoriously subject of strong debate. The question we tackled, although in an approximate
760 way, is if the surge model is capable to handle such a situation. The test we did, halting the wind at
761 the time of the documented front passage, showed a decrease of the sea level at the tower position,
762 but by only a fraction of what shown in Figure 15. We suspect that, fitted to the historical data,
763 hence without the cited particular situation, the model cannot handle this strong gradient situation.
764 We suspect this to be a characteristic of most costal surge models, and we put our data at disposal
765 for anyone keen to try his/her model in this rather unusual situation.

766 Maximum wave and crest heights

767 It is obviously of interest to be able, given the spectral conditions, to derive the expected maximum
768 wave and crest heights. We were able to verify our approach using the 13 UTC data, when both
769 video stereo record and model spectrum are available. Indeed the theoretically derived (from the
770 spectrum) maximum wave profile fits very well the measured one. We have then estimated the
771 corresponding profile for the heaviest conditions at 19. The resulting crest height (+7.90m) is
772 coherent with the damage reported at the tower. We are here close to the bottom induced limit
773 ($0.73 \times \text{depth}$, Battjes and Janssen, 1978), as suggested also by the shape of the previous and
774 following troughs. However, we believe such a limit cannot be taken as a drastic one. The point is
775 that there is a transient in approaching a breaking condition. Therefore, while true on average, we
776 do not consider the Battjes and Janssen limit as a physical barrier to the locally possible wave and
777 crest heights.

778

779 **11 - Summary**

780 We itemize our main findings as follows:

- 781 1) the storm of 29 October 2018 provided, despite its initial commonly observed structure, a rather
782 unusual development that led to extreme conditions on Northern Italy, in particular the Adriatic Sea,
- 783 2) the availability of detailed coastal and offshore observations in the Northern Adriatic Sea
784 provides a unique data-set allowing a keen study of the local physical processes,

785 3) the ECMWF winds are of high quality, but, as supported by previous studies, slightly
786 underestimated in the enclosed seas, in particular the Adriatic Sea. Regularly addressed in the local
787 operational activity on the base of long term comparisons, for this storm a posteriori the problem
788 has been eased by the availability of scatterometer data. We point out that the problem is not typical
789 of only the ECMWF data,

790 4) using the corrected winds from ECMWF forecasts, the wave and surge models provide results
791 consistent with the measured ones,

792 5) a non-negligible sea level difference is found between the tower and the coastal gauges (lower at
793 the tower). We associate this to the coastal set-up due to wave breaking and surface wind stress,

794 6) the data suggest that the passage of the cold front, with a consequent change of the surface wind
795 stress, leads to a sudden (order of minutes) collapse of the local sea level anomaly, both at the coast
796 and at the tower. Implicitly this offers the possibility of an indirect estimate of the surface wind
797 stress. However, a detailed analysis of the ensuing temporal and spatial variability will require a
798 much more detailed (kilometers and minutes) description of the local transient fields. We plan to
799 put the related data at disposal for tests by other models,

800 7) we found a good predictability of the storm, with substantial warnings up to 5 or 6 days ahead,
801 milder ones at 7 or 8 days ahead. The specific wind at the tower position, including gustiness, was
802 already high in the forecast of six or seven days ahead. However, this concerns more the general
803 pattern, hence the sirocco on the Adriatic Sea. It is less the case for the development of the
804 explosive cyclogenesis on the Western Mediterranean Sea.

805 8) we have evidence of reflected waves from the coast. The resulting partially standing waves are
806 associated to an enhanced seismometer signal recorded during the storm at Padua University, 40 km
807 inland.

808 9) the three highest storms in the last fifty years or so do not appear as possible extremes coherent
809 with long term historical distribution. Each one of them appears as the once in a while event. This is
810 unlikely. We suggest the possibility that they belong to a different family of events.

811

812 **Acknowledgements**

813 L.C.and L.B. highly appreciate the hospitality of ECMWF whose data have been essential for the
814 present study. All the meteorological data used in this study are the product of ECMWF. The maps
815 of Figures 2 and 11 have been plotted by Enrico Sambo of the CPSM (Tidal Forecast Center) in
816 Venice. The seismometer data have been provided by Andrea Battistella of Padua University whom
817 we thank for calling our attention on the matter. A.B. acknowledges the support from the
818 Copernicus Marine Environment Monitoring Service (CMEMS) LATEMAR project. The basic
819 image for Figure 2 has been provided by the SeaWiFS Project, NASA/Goddard Space Flight
820 Center, and ORBIMAGE. The one for Figure 3 has been taken from the NASA Earth Observatory
821 images by Jesse Allen and Robert Simmon, using Landsat data from the U.S. Geological Survey.
822 All the data and results used and reported in this paper are available from the authors. Following the

823 rules of the European Centre for Medium-Range Weather Forecasts, all the data derived from their
824 archive must be asked to the Centre.

825

826 **Declaration of interest:** none

827

828 **Contribution**

829 All the authors have contributed to both the scientific study and the preparation of the manuscript

830

831

832 **References**

833 Ardhuin, F., and A.Roland, 2012. Coastal wave reflection, directional spread, and seismoacoustic
834 noise sources, *J. Geoph. Res.*, Vol.117, C00120, 16pp, doi:10.1029/2011JC007832.

835 Bajo, M., I.Medugorac, U.Umgiesser, and M.Orlic, 2019. Storm surge and seiche modelling in the
836 Adriatic Sea and the impact on data assimilation, *Quart. J. Roy. Met. Soc.*, under minor
837 revision.

838 Battjes, J.A, and J.P.F.M.Janssen, 1978. Energy loss and set-up due to breaking random waves,
839 *Proceedings of 16th Conference on Coastal Engineering, Hamburg, Germany, 1978*

840 Benetazzo, A., F.Bergamasco, J.Yoo, L.Cavaleri, S.S.Kim, L.Bertotti, F.Barbariol, and J.S.Shim,
841 2018. Characterizing the signature of a spatio-temporal wind wave field, *Ocean Modelling*,
842 109, 104-123.

843 Benetazzo, A., Barbariol, F., Bergamasco, F., & Carniel, S. (2017). Space-time extreme wind
844 waves: Analysis and prediction of shape and height. *Ocean Modelling*, 113, 201–216.
845 <http://doi.org/10.1016/j.ocemod.2017.03.010>

846 Bertotti, L., and L.Cavaleri, 1985. Coastal set-up and wave breaking, *Oceanologica Acta*, Vol, 8, 2,
847 237-242.

848 Bertotti , P.Canestrelli, L.Cavaleri, F.pastore, and L.Zampato, 2011. The Henetus wave forecast
849 system in the Adriatic Sea, *Nat. Haz. And Earth Syst. Sc.*, 11(11), 2965-2979,
850 DOI:10.5194/nhess-11-2965-2011.

851 Bowen, A.J., D.L.Inman, and V.P,Simmons, 1968. Wave ‘set-down’ and set-up, *J. Geoph. Res.*,
852 Vol.73, 8, 2569-2577.

853 Cavaleri, L., 2000. The oceanographic tower Acqua Alta - activity and prediction of sea states at
854 Venice, *Coast. Eng.*, 39, 29-70

855

856 Cavaleri, L., and L.Bertotti, 2004. Accuracy of the modelled wind and wave fields in enclosed seas,
857 *Tellus*, 56A, 167-175.

858 Cavaleri L, Benetazzo A, Barbariol F, Bidlot JR, & Janssen PAEM. (2017). The Draupner event:
859 the large wave and the emerging view. *BULLETIN OF THE AMERICAN METEOROLOGICAL*
860 *SOCIETY*, 98, 729–735. <http://doi.org/10.1175/BAMS-D-15-00300.1>

861 Cavaleri, L., L. Bertotti, R. Buizza, A. Buzzi, V. Masato, G. Umgiesser, M. Zampieri, 2010:
862 Predictability of extreme meteo-oceanographic events in the Adriatic Sea. *Quart. J. Roy. Meteor.*
863 *Soc.*, **136**, 400-413.
864

865 ECMWF, 2018: Part VII : ECMWF Wave Model, IFS Documentation CY45R1, 7

866 Ferrarin, C., A.Cucco, G.Umgiesser, D.Bellafiore, and C.L.Amos, 2010. Modelling fluxes of water
867 and sediment between the Venice Lagoon and the sea, *Continental Shelf Research*, 30(8), 904–914.
868 <https://doi.org/10.1016/j.csr.2009.08.014>.

869 Ferrarin C., A.Roland, M.Bajo, G.Umgiesser, A.Cucco, S.Davolio, A.Buzzi, P.Malguzzi, and
870 O.Drofa, 2013. Tide-surge-wave modelling and forecasting in the Mediterranean Sea with focus on
871 the Italian coast. *Ocean Model.*, 61, 38-48.

872 Grazzini F. 2007. Predictability of a large-scale flow conducive to extreme precipitation over the
873 western Alps. *Meteorol. Atmos. Phys.* **95**: 123–138.

874 Janssen, P.A.E.M., 1991. Quasi-linear theory of wind-wave generation applied to wave forecasting,
875 *J. Phys. Oceanogr.*, 21, 11, 1631-1642.

876 Kedar, S., M.Longuet-Higgins, F.Webb, N.Graham, R.Clayton, and C.Jones, 2008. The origin of
877 deep ocean microseisms in the North Atlantic Ocean, *Proc. Royal Soc. A*, 464, 777-793,
878 doi:10.1098/rspa..2007.0277.

879 Komen, G.J., L.Cavaleri, M.Donelan, K.Hasselmann, S.Hasselmann and P.A.E.M.Janssen, 1994.
880 *Dynamics and Modelling of Ocean Waves*, Cambridge University Press, 532 pp.
881

882 Longuet-Higgins, 1951. A theory on the origin of microseisms, *Phil. Trans. Of the Roy. Soc. of*
883 *London, Series A*, Vol.243, 1-36.

884 Longuet-Higgins, M.S. and R.W.Stewart, 1964. Radiation stresses in water waves; a physican
885 discussion with applications, *Deep Sea Research*, 11, 529-562.

886 Madricardo, F., Foglini, F., Kruss, A., Ferrarin, C., Pizzeghello, N. M., Murri, C., et al., 2017:
887 High-resolution multibeam and hydrodynamic datasets of tidal channels and inlets of the Lagoon of
888 Venice. *Scientific Data*, 4, 170121. <https://doi.org/10.1038/sdata.2017.121>

889 Peureux, C., A.Benetazzo, and F.Ardhuin, 2018. Note on the directional properties of meter-scale
890 gravity waves, *Ocean Science*, 14, 41-52.

891 Pomaro, A, L.Cavaleri, and P.Lionello, 2018. 39 years of directional wave recorded data and
892 relative problems, climatological implications and use. *Scientific Data*, 5, 180139,
893 <https://doi.org/10.1038/sdata.2018.139>, with supplement dataset: Pomaro, A., L.Cavaleri, A.Papa,
894 P. Lionello, 2018. 39 years of directional wave recorded data at the Acqua Alta oceanographic
895 tower. PANGAEA, <https://doi.org/10.1594/PANGAEA.885361>

896 Rabier, F., H.Jarvinen, E.Klinker, J.-F.Mahfouf, and A.J.Simmons, 2007. The ECMWF operational
897 implementation of four-dimensional variational assimilation. I: Experimental results with simplified
898 physics, *Quart. Journ. of the Roy. Met. Soc.*, 126(564), 1143 – 1170.
899

- 900 Signell, R.P., S.Carniel, L.Cavaleri, J.Chiggiato, J.D.Doyle, J.Pullen, and M.Sclavo, 2005.
901 Assessment of wind quality for oceanographic modelling in semi-enclosed basins, *J. Mar. Syst.*,
902 Vol.53, 1-4, 217-233
- 903 Tayfun, M. A., & Fedele, F. (2007). Wave-height distributions and nonlinear effects. *Ocean*
904 *Engineering*, 34, 1631–1649.
- 905 Trincardi, F., A.Barbanti, M.Bastianini, A.Benetazzo, L.Cavaleri, J.Chiggiato, A.Papa, A.Pomaro,
906 M.Sclavo, L.Tosi, and G.Umgiesser, 2016. The 1966 flooding of Venice – what time taught us
907 for the future, *Oceanography*, 29(4), <https://doi.org/10.5670/oceanog.2016.87>.
- 908 Umgiesser G., C.Ferrari, A.Cucc, F.De Pascalis, D.Bellafiore, M.Ghezzo, and M.Bajo, 2014.
909 Comparative hydrodynamics of 10 Mediterranean lagoons by means of numerical modeling. *J.*
910 *Geophys. Res. Oceans*, 119(4), 2212-2226.
- 911

912 **Figure captions**

913 Figure 1 – Western and central Mediterranean Sea. The main geographical features and the relevant
914 locations are indicated. The lines show respectively: A) the path and timing of the cyclogenesis
915 minimum, B) the direction of the strong winds associated with it, C) the direction of the sirocco
916 winds on the Adriatic Sea, D) the path followed by the violent cold front. The small rectangle on
917 Venice indicates the area enlarged in Figure 3.

918 Figure 2 – Surface wind speed (ms^{-1}) and surface pressure fields on the Western Mediterranean Sea.
919 The four panels show the ECMWF analysis at respectively (UTC time of 29 and 30 October 2018):
920 a) 06-29, b) 12-29, c) 18-29, d) 00-30.

921 Figure 3 – Left panel: geometry of the area at the top of the Adriatic Sea (see Figure 1). The ‘tower’
922 is the position of the offshore structure shown in the right panel. Lido, Malamocco and Chioggia are
923 the three inlets connecting the sea with the lagoon. The Venice dot shows Punta Salute, the official
924 tide gauge for Venice floods.

925 Figure 4 – a) wind, b) wave, c) surge fields in the Adriatic Sea at 18 UTC of 29 October 2018.
926 Scales are respectively ms^{-1} , m, m.

927 Figure 5 – Left panel: ASCAT-B scatterometer data in the Adriatic Sea at 19.10 UTC 29 October
928 2018. Only part of the data is shown for better visibility. The right panel shows the best-fit between
929 ECMWF 10 m wind speeds and the ASCAT-B data.

930 Figure 6 – Comparison between wind speeds, significant wave heights and sea levels measured at
931 the tower (see Figure 3) and the corresponding model data. Time (hours) goes from 00 UTC of 29
932 till 12 UTC of 30 October 2018.

933 Figure 7 – Hourly wave spectra at the oceanographic tower. See its position in Figure 3. Left panel:
934 measured spectra, right one: model spectra. The thin lines show the obvious growing stages of the
935 storm. The thick line is the peak condition. The dotted lines show the progressively decreasing
936 stages.

937 Figure 8 – 2D spectra at the oceanographic tower. See Figure 3 for its position. Left, measured
938 spectrum (with the video stereo system); right, model spectrum. Note the opposite going waves in
939 the measured spectrum.

940 Figure 9 – Astronomical tide, surge and total sea level at the oceanographic tower. See Figure 3 for
941 its position. Time (hours) goes from 00 UTC of 29 till 12 UTC of 30 October 2018. The blue line
942 shows the model surge. The actual 0 of the astronomical tide is 26.3 cm above the official reference
943 for Venice. See text for explanation.

944 Figure 10 - The box-and-whisker plot shows the evolution of forecasts for 24-hour maximum wind
945 gusts on 29 October for the location of the tower for different starting dates. See Figures 1 and 3 for
946 its position. The blue (red) bars indicate the 1st, 10th, 25th, 75th, 90th and 99th percentile for the
947 ensemble forecast (model climate of the ensemble), and the red dot the HRES forecast. The black

948 dots are the mean of the respective distributions. The 32 ms^{-1} dashed line is the peak gust recorded
949 at the tower.

950 Figure 11 – Adriatic Sea. See Figure 1 for its position. Wind fields at 18 UTC 29 October 2018
951 according to the forecasts issued respectively at 00 UTC of a) 24, b) 25, c) 26, d) 27, e) 28, f) 29
952 October 2018.

953 Figure 12 – Predictability of the 29 October 2018 event. The two panels show the corresponding
954 surge and significant wave height forecasts issued at different dates and time. The horizontal bars
955 show the errors in timing the worst 29 October 19 UTC conditions. The two horizontal dashed lines
956 show the respective measured values.

957 Figure 13 – Sea level at the coast (Lido inlet) and the tower. See Figure 3 for their position. The
958 other two lines show the respective difference (coastal set-up) and the significant wave height at the
959 tower. Time (hours) goes from 00 UTC of 29 till 12 UTC of 30 October 2018.

960 Figure 14 – Modeled sea level distribution at 18 UTC 29 October 2018 in the area off the Venice
961 coastline and in the lagoon. See Figures 1 and 3 for their position. The small circle shows the tower
962 position.

963 Figure 15 – Time history (17-21 UTC 29 October 2018) of the recorded sea level at the tower (ptf)
964 and Lido and Chioggia inlets. See Figure 3 for their positions.

965 Figure 16 – Left panel: original output (29-30 October 2018) of the seismometer at Padua
966 University, 40 km inland with respect to the coast. To the right: spectrum at the time of the red
967 dashed line..

968 Figure 17 - Largest wave heights. Left panel: normalized profile of the expected largest wave at the
969 tower at 13 UTC, from stereo observations (black dashed line) and model estimate (blue solid line).
970 Space and time intervals considered are 35 m^2 and 120 s. The gray region represents the confidence
971 limit of the observations. Right panel: profile of the wave with the largest expected crest height at
972 19 UTC, from model estimate, compared to the highest tower deck that was damaged. Space and
973 time intervals considered are 35 m^2 and 3600 s. Sea level at the time was 1.00 m.
974

975 Figure 18 – Largest wave heights. Left panel: exceedance distribution function (EDF) of the
976 observed crest heights (data, blue dots), from the single point radar (3600 s). Theoretical EDFs are
977 plotted for reference (R: Rayleigh, T: Tayfun, TF: Tayfun-Fedele). Right panel: profile of the wave
978 with the largest crest height, compared to the highest tower deck where damaged was reported. Sea
979 level at the time was 0.94 m.
980

981 Figure 19 – Statistical distributions of the maxima surge η and significant wave height H_s values for
982 all the events for $\eta > 0.5 \text{ m}$ and $H_s > 2.0 \text{ m}$. The period considered is 1979 to present.

983

984